

1 **A novel gain-of-function sodium channel β 2 subunit mutation in idiopathic small**
2 **fiber neuropathy**

3 Matthew Alsaloum^{1,2,3,4,5}, Julie Labau^{1,2,3,6,9}, Daniel Sosniak^{1,2,3}, Peng Zhao^{1,2,3}, Rowida
4 Almomani^{6,7}, Monique Gerrits⁸, Janneke G.J. Hoeijmakers⁹, Giuseppe Lauria^{10,11},
5 Catharina G. Faber⁹, Stephen G. Waxman^{1,2,3}, Sulayman Dib-Hajj^{1,2,3}

6
7 ¹Department of Neurology, Yale University School of Medicine, New Haven, CT, USA.

8 ²Center for Neuroscience & Regeneration Research, Yale University, West Haven, CT,
9 USA.

10 ³Center for Rehabilitation Research, VA Connecticut Healthcare System, West Haven,
11 CT, USA.

12 ⁴Yale Medical Scientist Training Program, Yale School of Medicine, New Haven, CT,
13 USA.

14 ⁵Interdepartmental Neuroscience Program, Yale School of Medicine, New Haven, CT,
15 USA.

16 ⁶Department of Genetics and Cell Biology, Clinical Genomics Unit, Maastricht
17 University, Maastricht, the Netherlands

18 ⁷Department of Medical Laboratory Sciences, Jordan University of Science and
19 Technology, Irbid, Jordan

20 ⁸Department of Clinical Genetics, Maastricht University Medical Centre+, Maastricht, the
21 Netherlands

22 ⁹Department of Neurology, Maastricht University Medical Centre+, Maastricht, the
23 Netherlands

24 ¹⁰Neuroalgology Unit, IRCCS Foundation "Carlo Besta" Neurological Institute, Milan,
25 Italy

26 ¹¹Department of Biomedical and Clinical Sciences "Luigi Sacco," University of Milan,
27 Milan, Italy

28
29 Corresponding author:
30 Sulayman D. Dib-Hajj, PhD
31 Neuroscience and Regeneration Research Center
32 VA Connecticut Healthcare System
33 950 Campbell Avenue, Bldg. 34
34 West Haven, CT 06516
35 Email: sulayman.dib-hajj@yale.edu
36

37

38 **Abstract**

39 Small fiber neuropathy (SFN) is a common condition affecting thinly myelinated A δ and
40 unmyelinated C fibers, often resulting in excruciating pain and dysautonomia. SFN has
41 been associated with several conditions, but a significant number of cases have no
42 discernible cause. Recent genetic studies have identified potentially pathogenic gain-of-
43 function mutations in several the pore-forming voltage-gated sodium channel α subunits
44 (Na_vs) in a subset of patients with SFN, but the auxiliary sodium channel β subunits
45 have been less implicated in the development of the disease. β subunits modulate Na_v
46 trafficking and gating, and several mutations have been linked to epilepsy and cardiac
47 dysfunction. Recently, we provided the first evidence for the contribution of a mutation in
48 the $\beta 2$ -subunit to pain in human painful diabetic neuropathy.

49 Here, we provide the first evidence for the involvement of a sodium channel β subunit
50 mutation in the pathogenesis of SFN with no other known causes. We show, through
51 current-clamp analysis, that the newly-identified Y69H variant of the $\beta 2$ subunit induces
52 neuronal hyperexcitability in dorsal root ganglion neurons, lowering the threshold for
53 action potential firing and allowing for increased repetitive action potential spiking.
54 Underlying the hyperexcitability induced by the $\beta 2$ -Y69H variant, we demonstrate an
55 upregulation in tetrodotoxin-sensitive, but not tetrodotoxin-resistant sodium currents.
56 This provides the first evidence for the involvement of $\beta 2$ subunits in SFN and
57 strengthens the link between sodium channel β subunits and the development of
58 neuropathic pain in humans.

59

60 **New & Noteworthy**

61 Small fiber neuropathy (SFN) often has no discernible cause, although mutations in the
62 voltage-gated sodium channel α -subunits have been implicated in some cases. We
63 identify a patient suffering from SFN with a mutation in the auxiliary β 2-subunit and no
64 other discernible causes for SFN. Functional assessment confirms this mutation renders
65 dorsal root ganglion neurons hyperexcitable and upregulates tetrodotoxin-sensitive
66 sodium currents. This study strengthens a newly-emerging link between sodium
67 channel β 2-subunit mutations and human pain disorders.

68

69

70 **Introduction**

71 Small-fiber neuropathy (SFN) is a painful condition selectively affecting thinly
72 myelinated A δ -fibers and unmyelinated C-fibers(1). Clinically, SFN often presents with
73 chronic pain, usually described as “burning” and in a “glove and stocking” distribution,
74 dysautonomic symptoms, no signs of large-diameter fiber involvement, and reduced
75 intraepidermal nerve fiber density on skin biopsy(2-5). The sequelae of SFN are
76 associated with significant reductions in patient quality of life(6). Additionally, worsening
77 SFN pain is also directly associated with worse mental health, sleep, and employment
78 outcomes(7). Current first-line therapeutic strategies for the management of chronic
79 pain associated with painful neuropathy, including SFN, are not very effective, in part
80 due to adverse effects(8, 9). More effective pharmacological management is thus a high
81 priority, and a better understanding of underlying causes of pain may provide more
82 effective treatment options.

83 Many causes of SFN have been identified(10-12), including autoimmune conditions,
84 sodium channel gene mutations(1, 13-16), diabetes mellitus(17), and
85 chemotherapy(18). However, a significant proportion of patients with SFN have no
86 identifiable cause, termed idiopathic small-fiber neuropathy (I-SFN)(10, 19). Knowledge
87 of the etiology underlying SFN is important as some conditions are preventable or can
88 be targeted with a precision medicine approach(20).

89 Mutations in sodium channel genes are responsible for a sizable percentage of SFN
90 cases (11.6 %)(16), which is explicable as voltage-gated sodium channels (Na_vs) play a
91 pivotal role in regulating neuronal excitability(21, 22). Sodium channels are composed
92 of a pore-forming α -subunit (Na_v) which is associated with auxiliary β subunits(23). Nine

93 different Na_V s ($\text{Na}_V1.1$ - $\text{Na}_V1.9$) are expressed in humans(24). $\text{Na}_V1.7$, $\text{Na}_V1.8$, and
94 $\text{Na}_V1.9$ are preferentially expressed in the developed peripheral nervous system and
95 have been genetically and functionally well-validated as drivers of chronic pain in
96 humans(25-27). $\text{Na}_V1.7$ was the first Na_V channel linked directly to pain, with gain-of-
97 function mutations resulting in a variety of pain conditions, including inherited
98 erythromelalgia(28-32), paroxysmal extreme pain disorder, and SFN(1). Loss-of-
99 function mutations result in congenital insensitivity to pain(33-35). Subsequently, other
100 Na_V s were found to play pivotal roles in SFN, including both $\text{Na}_V1.8$ (13, 36) and
101 $\text{Na}_V1.9$ (15). However, while the contribution of Na_V s to painful neuropathies has been
102 thoroughly investigated, the contributions of sodium channel β subunits to pain are still
103 being elucidated.

104 The sodium channel β -subunit family is comprised of four genes, *SCN1B-SCN4B*,
105 encoding four distinct proteins, $\beta1$ - $\beta4$, and two splice variants, $\beta1A$ and $\beta1B$ (37, 38).
106 Na_V s are found as heterotrimeric complexes *in vivo*, consisting of one pore-forming α -
107 subunit ($\text{Na}_V1.1$ - $\text{Na}_V1.9$) and two non-ion conducting β -subunits ($\beta1/3$ and $\beta2/4$)(39, 40).
108 β -subunits play important roles in a number of cellular and molecular processes. For
109 example, β -subunits are known to alter the biophysical properties of multiple Na_V α -
110 subunits(41-44). They also are important for normal Na_V localization and membrane
111 trafficking(44-49). Additionally, β -subunits act as cell adhesion molecules(50) and are
112 implicated in multiple diseases of the cardiac conducting system(51, 52) and
113 epilepsy(53-56). Given the multiple roles of sodium channel β -subunits in Na_V
114 modulation, it is unsurprising that their upregulation has been linked to neuropathic pain,
115 while their knock-out or knockdown ameliorates pain in preclinical rodent models(57,

116 58). Only recently, though, has a mutation in a β -subunit (β 2-D109N) been linked to
117 pain in a patient with painful diabetic neuropathy(59). Functional analysis showed that
118 the D109N mutation caused a depolarizing shift in the voltage-dependence of $\text{Na}_v1.7$
119 fast-inactivation and reduced use-dependent inhibition of the $\text{Na}_v1.7$ channel, enhancing
120 dorsal root ganglion (DRG) neuronal action potential firing, consistent with its
121 contribution to pain in this patient. Here, we present the case of a novel β 2-subunit
122 mutation involved in the development small-fiber neuropathy with no other underlying
123 pathophysiology. The newly identified Y69H variant increases tetrodotoxin-sensitive
124 (TTX-S) current density, without altering Na_v gating properties, enhancing the
125 excitability of DRG neurons. Our data expands the role of β 2 subunit mutations at the
126 sodium channel level and strengthens the evidence for a role of these subunits in
127 human pain disorders.

128

129 **Materials and Methods**

130 *DNA isolation from peripheral blood*

131 Local medical ethical committees at each of the participating centers approved this
132 study. Written informed consent by patients was obtained prior to participation in this
133 study. A peripheral blood sample was taken from all patients in a cohort with SFN(59)
134 and genomic DNA was extracted from peripheral blood using either a QIAamp DNA
135 Blood Maxi Kit/Puregene Blood Core Kit (Qiagen, Hilden, Germany) or a NucleoSpin 8
136 Blood Isolation Kit (Macherey-Nagel, Düren, Germany). Quality and concentration of the
137 DNA were determined by NanoDrop (Thermo Scientific, Wilmington, DE, USA) and
138 Qubit 2.0 Fluorometer using the Qubit® dsDNA BR assay kit (Life technologies,
139 Bleiswijk, The Netherlands). Isolated DNA was stored with a unique numeric code in the
140 central DNA bank at Maastricht University Medical Centre and IRCCS Foundation
141 “Carlo Besta” Neurological Institute.

142 *Single-molecule molecular inversion probe-next-generation sequencing*

143 Genetic sequencing was conducted as previously described(60). In brief, coding exons
144 and exon-flanking intron sequences (± 20 bp) of *SCN1B-4B*, *SCN3A*, and *SCN7A-11A*
145 were sequenced by single-molecule molecular inversion probe-next-generation
146 sequencing (smMIP-NGS). Three-hundred-twenty-four smMIPs were designed using a
147 modified version of MIPgen software (<http://shendurelab.github.io/MIPGEN/>). The gap
148 fill length between the extension and ligation arm (region of interest) of the smMIPs was
149 fixed to 220–230 nucleotide. Probes were synthesized by Integrated DNA Technologies
150 (IDT, Iowa, IA, USA).

151 To identify sequence variations in *SCN1B-4B*, *SCN3A*, *SCN7A-11A*, patients' coding
152 and immediate flanking regions of these genes were compared with reference
153 sequence GRCh37. Genetic variations detected were annotated according to the
154 guidelines of the Human Genome Variation Society (<http://www.hgvs.org/mutnomen/>).
155 Variants with a possible pathogenic effect were classified using Alamut Mutation-
156 Interpretation Software (Interactive-Biosoftware, Rouen, France). Classification of
157 variants was based on the practice guidelines of the Association for Clinical Genetic
158 Science.

159 *Isolation and transfection of DRG neurons*

160 The Y69H mutation was introduced into the plasmid encoding wild-type human- β 2-
161 IRES-GFP(61) using QuickChange Lightning site-directed mutagenesis (Agilent, Santa
162 Clara, CA). All animal studies and procedures followed a protocol that was approved by
163 the Veterans Administration Connecticut Healthcare System Institutional Animal Care
164 and Use Committee. DRG neurons from 4- to 6- week old Sprague-Dawley rats of both
165 sexes were harvested and dissociated as described previously with minor
166 differences(62). In brief, adult rat DRGs were dissociated with a 20- minute incubation in
167 1.5 mg/mL collagenase A (Roche, Indianapolis, IN, USA) and 0.6 mM EDTA, followed
168 by a 17-minute incubation in 1.5 mg/mL collagenase D (Roche), 0.6 mM EDTA, and 30
169 U/mL papain (Worthington Biochemical, Lakewood, NJ, USA). DRGs were then
170 centrifuged and triturated in 0.5 mL of DRG media (DMEM/F12 with 100 U/ml penicillin,
171 0.1 mg/ml streptomycin, and 10% fetal bovine serum) containing 1.5 mg/mL bovine
172 serum albumin (low endotoxin) and 1.5 mg/mL trypsin inhibitor (Sigma, St. Louis, MO,
173 USA). After trituration, undigested tissue was filtered using a 70- μ m cell strainer (Becton

174 Dickinson, Franklin Lakes, NJ, USA). The mesh was washed twice with 2 mL of DRG
175 media. Neurons were then pelleted and transfected with either human- β 2-Y69H or
176 human- β 2-wild type (WT) cDNA carrying an internal ribosome entry site (IRES)-GFP to
177 mark transfected cells using a Nucleofector IIS (Lonza, Basel, Switzerland) and Amaxa
178 Basic Neuron SCN Nucleofector Kit (VSPI-1003).

179 *HEK293 stable cell line transfection*

180 Human embryonic kidney (HEK293) cells stably expressing a tetrodotoxin-resistant
181 version of the $\text{Na}_v1.7$ channel were transfected with either 0.5 $\mu\text{g}/\mu\text{L}$ of human β 2-Y69H
182 or human β 2-WT cDNA containing an internal ribosome entry site (IRES)-GFP tag using
183 a LipoJet transfection kit (SignaGen Laboratories, Rockville, MD, USA). The cells were
184 grown and maintained under standard culture conditions (37°C, 5% CO₂) in Dulbecco's
185 modified Eagle's medium (DMEM/F12), supplemented with 10% fetal bovine serum
186 (FBS) and 1% penicillin/streptomycin. Transfected cells were grown in 35 mm dishes,
187 before being resuspended and plated onto PDL/laminin-coated coverslips the next day.
188 Sodium currents were recorded 24-48 hours following transfection.

189 *Macroscopic current recordings*

190 Macroscopic currents were recorded from adult rat DRG neurons in both current-clamp
191 and voltage-clamp configurations using an EPC-10 amplifier and the PatchMaster
192 program (HEKA Elektronik, Holliston, MA, USA) at room temperature. Patch pipettes
193 were pulled from borosilicate glass (1.65 mm/1.1 mm outside diameter/inside diameter;
194 World Precision Instruments, Sarasota, FL, USA) using a Sutter Instruments P-97 puller
195 and had a resistance of 0.6-1.8 M Ω .

196 For current-clamp recordings, the extracellular solution contained (in mM): 140 NaCl, 3
197 KCl, 2 MgCl₂, 2 CaCl₂, and 10 HEPES. Patch pipettes were filled with intracellular
198 solution containing (in mM): 140 KCl, 3 Mg-ATP, 0.5 EGTA, 5 HEPES, and 30 dextrose.
199 Both solutions were titrated to a pH of 7.3 with NaOH and KOH, respectively, and
200 brought to a final osmolarity (320 and 310 mOsm for extracellular and intracellular
201 solutions, respectively) using dextrose. Whole-cell configuration was obtained in
202 voltage-clamp mode before transitioning to current-clamp mode. Fluorescent small DRG
203 neurons (<30 μm diameter) with stable (<10% variation) resting membrane potentials
204 (RMPs) and minimal leak currents at break-in were included in the analysis. Cells with
205 an input resistance lower than 100 MΩ were excluded from analysis. Input resistance
206 was calculated as the slope of the linear fit of the hyperpolarizing response to current
207 steps from -5 pA to -40 pA in 5 pA increments.

208 In current-clamp mode, rheobase was defined as the first current injection step that
209 resulted in action potential firing without further failure and was determined by a series
210 of depolarizing current injections (200 ms) that increased incrementally by 5 pA. For the
211 calculation of rheobase, action potentials were defined as rapid increases in membrane
212 potential to >40 mV with a total amplitude >80 mV. However, as neurons often
213 attenuate firing with repetitive action potential spiking, when examining repetitive firing,
214 action potentials were counted if the membrane potential rapidly crossed 0 mV,
215 regardless of overshoot or total amplitude. Action potential repetitive firing frequency
216 was determined by quantifying the number of action potentials that a neuron fired during
217 a 500 ms current injection at current injections between 25 and 500 pA, in 25 pA steps.

218 For voltage-clamp recordings, the extracellular bath solution contained (in mM) 140
219 NaCl, 20 TEA-Cl, 3 KCl, 1 CaCl₂, 1 MgCl₂, 5 CsCl, 0.1 CdCl₂, and 10 HEPES (± 0.1
220 tetrodotoxin [TTX]), titrated to a pH of 7.3 using NaOH. Patch microelectrodes contained
221 an intracellular solution consisting of (in mM): 140 CsF, 10 NaCl, 1.1 EGTA, and 10
222 HEPES, titrated to a pH of 7.3 using CsOH. Both solutions were brought to final
223 osmolality (320 mOsm for extracellular solution and 310 mOsm for intracellular solution)
224 using dextrose.

225 Sodium currents from fluorescent (indicating successful transfection) DRG neurons
226 under 30 μm in diameter were recorded in the whole-cell configuration. For biophysical
227 analysis of sodium channel gating, series resistance prediction and compensation
228 (60%-90%) were applied to reduce the voltage errors. Neurons with a peak voltage
229 error greater than 5 mV were excluded from all biophysical analyses. The recorded
230 currents were digitized at a rate of 50 kHz after passing through a low-pass Bessel filter
231 setting of 10 kHz. After achieving whole-cell configuration, a 5-minute equilibration
232 period was allowed before starting the recording. DRGs were held at -100 mV to
233 minimize inactivation of Na_v1.9 while maintaining neuronal cell viability.

234 To measure sodium channel activation, DRG neurons were pulsed to a range of
235 potentials between -80 mV and +30 mV, in 5 mV increments, for 100 ms after being
236 held at a holding potential of -100 mV. Peak inward currents were transformed to
237 conductance using the equation $G = \frac{I_{Na}}{V_m - E_{Na}}$. Reversal potentials were calculated in the
238 FitMaster program (HEKA Elektronik). The conductance at each voltage was
239 normalized to the maximum conductance and fit with the following Boltzmann equation

240 to derive the activation curve: $G = \frac{G_{min} + (G_{max} - G_{min})}{1 + e^{((V_{0.5} - V_m)/K)}}$, where $V_{0.5}$ is the half-maximal
241 activation potential and k is the slope factor of the activation curve.

242 Use-dependent inhibition at 20 Hz stimulation was determined by holding the neurons at
243 -80 mV for 2 ms, followed by a 10 ms step to -20 mV and measuring the charge transfer
244 through the cell. Use-dependence curves were generated by normalizing the current
245 passed at each sweep to the current passed at the first sweep.

246 To assess steady-state fast-inactivation, DRG neurons were prepulsed to a range of
247 voltages between -140 mV and 0 mV in 10 mV steps for 500 ms from a holding potential
248 of -100 mV and then pulsed to a potential of -10 mV. Peak inward current was
249 normalized to the maximum peak inward current and fit with the following double
250 Boltzmann equation to derive the inactivation curve:

$$251 \quad I = I_{min} + A \left[\frac{p}{1 + e^{\frac{x - x_{01}}{k_1}}} + \frac{1 - p}{1 + e^{\frac{x - x_{02}}{k_2}}} \right].$$

252 To assess deactivation, DRG neurons were activated by a brief 0.5 ms pulse to -10 mV
253 from a holding potential of -120 mV. Following this brief activation step, the kinetics of
254 deactivation were examined by 50 ms pulses at a range of potentials from -40 mV to -
255 120 mV in -5 mV increments. The tail-currents were fit with a single exponential
256 equation in order to derive the time constant of decay.

257 To assess recovery from fast-inactivation, we utilized a two-pulse protocol (both to -10
258 mV) with varied interpulse interval between 1 and 513 ms at voltage potentials between
259 -120 mV and -70 mV. The current evoked by the test pulse at -10 mV was normalized to
260 the current elicited by the prepulse at -10 mV to represent the fraction of recovering

261 currents. This was then plotted against the interpulse duration to calculate the rate and
262 extent of recovery from inactivation.

263 Peak current density was calculated as the peak current during the activation pulse
264 (described above) normalized to the cellular capacitance. To assess tetrodotoxin-
265 resistant (TTX-R) and TTX-S currents, 1 μ M tetrodotoxin (TTX) was applied. Total
266 sodium currents were recorded prior to TTX application. Extracellular bath solution
267 containing 1 μ M TTX was subsequently perfused into the chamber while continuously
268 suctioning the chamber. In order to ensure full solution exchange, at least 5X the total
269 volume of the chamber of solution was perfused. Additionally, test pulses to -10 mV
270 were conducted until the current no longer decreased. TTX-R currents were
271 subsequently recorded. To calculate TTX-S currents, reference series subtraction in
272 PatchMaster was utilized.

273 *Molecular modeling*

274 Protein data bank (PDB) structure 6J8I from Shen *et al.*(39) was downloaded from
275 RCSB.org and embedded in a heterogeneous lipid bilayer using CHARMM-GUI(63) to
276 reflect a more physiologically relevant background. The structure was then edited in
277 PyMol (Schrödinger, LLC).

278 *Data Analysis*

279 All data are represented as mean \pm standard error of the mean, unless otherwise noted.
280 All Boltzmann fits and graphical representation was conducted in GraphPad Prism.
281 Significance in figures is noted as * ($p \leq 0.05$), ** ($p \leq 0.01$), or *** ($p \leq 0.001$).

282

283 **Results**

284 *Identification of a novel variant in the coding region of the SCN2B gene*

285 In our cohort of 548 patients diagnosed with painful SFN and no other underlying
286 causes, MIPs-NGS identified two potentially pathogenic novel *SCN2B* gene variants
287 that were found only in patients with painful SFN and not in any patients with painless
288 conditions. Of these variants, one (c.502G>T; pG168C) was in the transmembrane
289 segment of $\beta 2$, whereas the second (c.205T>C; pY69H), a tyrosine-to-histidine
290 missense mutation at position 69 resides in the immunoglobulin domain of the protein
291 (Figure 1). The rare Y69H variant, classified as a variant of unknown significance(64)
292 with an allele frequency of 4.95×10^{-5} , was initially chosen for investigation because it
293 had also been identified in patients with Brugada syndrome and one patient with chronic
294 atrial fibrillation(65). Additionally, the only previously characterized mutation in the
295 sodium channel $\beta 2$ subunit associated with a painful neuropathy was also located in the
296 immunoglobulin domain(59).

297 The $\beta 2$ -Y69H variant was identified in a patient with painful idiopathic SFN presenting
298 as a stabbing and burning pain in both legs, as well as red discoloration of the soles of
299 her feet, beginning at age 53. She was assessed clinically and her neurologic physical
300 exam was normal. She also had normal nerve conduction studies, consistent with
301 unaffected large, myelinated nerve fibers. Thermal testing showed abnormal warmth
302 and cold sensation, and reduced intraepidermal nerve fiber density (1.1 per mm, with a
303 lower limit of normal accepted at 4.3 per mm). There was no other relevant medical
304 history that could potentially explain her peripheral neuropathy. Cardiovascular workup
305 was normal and no prior history of cardiovascular disease was noted.

306 Electrocardiogram conducted at the time showed sinus rhythm with normal conduction
307 times; the PR interval spanned 154 ms (normal limits: 120-200 ms), the QRS complex
308 spanned 86 ms (normal limits: 60-100 ms), and the QT interval spanned 464 ms, with a
309 corrected QT (QTc) interval of 401 ms (99th percentile QTc in post-pubertal females:
310 480 ms). No other *SCN1B-4B*, *SCN3A*, or *SCN7A-11A* variants, others than the *SCN2B*
311 Y69H variant, were detected by MIPs-NGS; she was heterozygous for the *SCN2B*
312 Y69H variant.

313 *Human β 2-Y69H confers hyperexcitability on DRG neurons*

314 To test whether the Y69H variant contributes to enhanced neuronal excitability, DRG
315 neurons were isolated from adult rats and transfected with either wild-type human β 2 or
316 the β 2-Y69H variant. Excitability of DRG neurons was analyzed by current-clamp
317 recordings. We examined passive membrane properties, such as the neuronal RMP
318 (Figure 2A). The RMP of neurons expressing the β 2-Y69H variant (-48.21 ± 1.99 mV, n
319 = 11) was not statistically different from that of neurons expressing the wild-type β 2
320 subunit (-50.18 ± 2.48 mV, n = 11, two-tailed Student's t-test p = 0.54). Additionally,
321 input resistances of non-spontaneously firing DRG neurons were comparable between
322 those expressing the wild-type β 2 subunit (732.95 ± 130.13 M Ω , n = 11) and those
323 expressing the Y69H variant (959.70 ± 97.82 M Ω , n = 11, Student's t-test p = 0.18).
324 Neurons expressing the β 2-Y69H variant were more excitable at rest than neurons
325 exhibiting the wild-type β 2 subunit (Figure 2B), with a numerically larger percentage of
326 neurons firing spontaneous action potentials; 47.62% of neurons expressing the Y69H
327 variant fired action potentials spontaneously, compared to only 21.42% of neurons
328 expressing the wild-type β 2 subunit. However, this study was not powered to detect

329 spontaneous action potential firing and was therefore not statistically significant
330 (Fisher's exact test, $p = 0.16$).

331 Neurons expressing the $\beta 2$ -Y69H variant are significantly more excitable in response to
332 current injection stimuli than neurons expressing the wild-type $\beta 2$ subunit. We examined
333 the current injection necessary to evoke an action potential in adult rat DRG neurons
334 (Figure 3A, 3B). Rheobase (Figure 3B) was significantly lower in neurons expressing
335 the Y69H variant (51.36 ± 53.81 pA, $n = 11$) compared to neurons expressing the wild-
336 type $\beta 2$ subunit (163.64 ± 47.85 pA, $n = 11$, Student's t-test, $p = 0.038$). Furthermore,
337 neurons expressing the Y69H variant were capable of significantly increased repetitive
338 action potential firing, compared to neurons expressing the wild-type $\beta 2$ variant (Figure
339 3C, 3D, 3E). When each neuron was injected with a 1-second current stimulus at the
340 amplitude that was sufficient to stimulate an action potential at 200-millisecond duration,
341 to the nearest 25 pA, neurons expressing the wild-type $\beta 2$ subunit fired significantly
342 fewer action potentials (0.73 ± 0.47 , $n = 11$) than did neurons expressing the Y69H
343 variant (3.82 ± 1.01 , $n = 11$, two-tailed Student's t-test $p = 0.0065$, Figure 3C). In
344 response to graded current injections from 25 pA to 500 pA in 25 pA increments,
345 neurons expressing the Y69H variant fired significantly more action potentials across
346 the entire stimulus range (two-way repeated measures ANOVA, $p = 0.004$). This
347 difference was statistically significant after correcting for multiple comparisons using the
348 Holm-Šídák method at 150, 175, 200, 225, and 275 pA current injections (Figure 3E).

349 *Biophysical analysis of the $\beta 2$ -Y69H variant on total sodium current*

350 We investigated mechanisms underlying the hyperexcitability of DRG neurons
351 expressing the $\beta 2$ -Y69H variant using voltage-clamp recordings to study voltage-

352 dependent sodium currents. We examined the biophysical properties of the total sodium
353 current passed by DRG neurons transfected with either wild-type $\beta 2$ or $\beta 2$ -Y69H
354 plasmids (Figure 4). The Y69H variant did not significantly alter the half-maximal voltage
355 of activation ($V_{1/2}$, -21.04 ± 1.40 mV, $n = 18$) for total sodium current compared to
356 neurons expressing the wild-type $\beta 2$ subunits (-16.78 ± 2.18 mV, $n = 15$, Student's t-test
357 $p = 0.10$), although the point estimates showed an approximately 4.3 mV
358 hyperpolarization (Figure 4A). Similarly, the slope of the activation curves showed a
359 trend towards faster activation of sodium current in neurons expressing the Y69H
360 variant (6.37 ± 0.45 ms, $n = 18$) compared to wild-type (8.72 ± 1.20 ms, $n = 15$,
361 Student's t-test $p = 0.059$). In addition to activation, we also examined the effect of the
362 variant $\beta 2$ subunit on sodium current inactivation (Figure 4A). Current traces were best
363 fit with a double Boltzmann equation and showed no difference in the $V_{1/2}$ of fast-
364 inactivation or the slope for the development of fast-inactivation between the Y69H
365 variant and the wild-type subunit (Table 1).

366 The Y69H variant caused no reduction in total sodium current use-dependent inhibition
367 (Figure 4B); after 1.5 seconds of 20 Hz pulses to -20 mV, neurons expressing the wild-
368 type human $\beta 2$ subunit passed 76.12% of the current passed during the first stimulus,
369 which was comparable to neurons expressing the Y69H variant (74.85%). Likewise,
370 neurons expressing either construct showed a similar extent of channel recovery
371 (Figure 4C) and there was no change in the rate of recovery from fast-inactivation
372 between neurons expressing the wild-type and the Y69H variant (Figure 4D). Finally, we
373 assessed the rate of channel deactivation (Figure 4E) and found no change between
374 DRG neurons expressing the wild-type or Y69H variant $\beta 2$ subunit.

375 *Tetrodotoxin-sensitive currents are upregulated by the β 2-Y69H variant*

376 Given that there were no major biophysical changes conferred on sodium channels by
377 the Y69H variant β 2 subunit, we then examined sodium channel current density as the
378 β -subunits are known to enhance channel trafficking to the plasma membrane(44, 66).
379 DRG neurons were held at -100 mV and then pulsed to a range of potentials from -80
380 mV to + 30 mV for 100 ms in 5 mV increments and the current density was calculated at
381 each step pulse. Neurons expressing the Y69H variant exhibited a significantly larger
382 peak total sodium current density (-590.90 ± 46.21 pA/pF, $n = 21$) after a 100 ms pulse
383 compared to DRG neurons expressing the wild-type β 2 subunit (-359.11 ± 36.11 pA/pF,
384 $n = 17$, Student's t-test $p = 0.00052$, Figure 5B). Additionally, as current density is
385 derived from both the amplitude of the currents, as well as the capacitance of the
386 neurons, we sought to confirm that there was no difference in the capacitance of the
387 cells recorded. The capacitance of DRG neurons expressing the Y69H variant β 2
388 subunit (22.91 ± 2.05 pF, $n = 21$) was similar to that of DRG neurons expressing the
389 wild-type subunit (21.80 ± 2.42 pF, $n = 17$, Student's t-test $p = 0.73$).

390 We next sought to determine whether the upregulated sodium currents were TTX-S or
391 TTX-R. The same voltage protocol as above was applied first in the absence of TTX,
392 then after perfusion of 1 μ M into the recording chamber. TTX-S current was calculated
393 by reference series subtraction of TTX-R current from the total sodium current (Figure
394 5A). It is important to note that a voltage error greater than 5 mV was an exclusion
395 criterion in the first set of experiments to minimize uncertainty in biophysical analysis of
396 channel gating. In this second set of experiments, however, voltage error was not
397 considered. This was a decision consciously made in order to avoid artificially limiting

398 any difference between the wild-type and Y69H-expressing neurons by excluding cells
399 with large currents. Crucially, voltage error would not affect the determination of sodium
400 current density. We were able to confirm again, in this second set of experiments, an
401 upregulation of total Na_v current in DRG neurons expressing the Y69H variant
402 compared to DRG neurons expressing the wild-type variant (Y69H: -879.82 ± 261.94
403 pA/pF, $n = 15$; wild-type: -435.02 ± 69.42 pA/pF, $n = 26$; Student's t-test $p = 0.048$).
404 However, we did not detect a statistically significant difference in TTX-R current in cells
405 expressing the YH variant (-214.273 ± 44.81 pA/pF, $n = 15$) compared to DRG neurons
406 expressing the wild-type variant (-189.30 ± 32.47 pA/pF, $n = 26$, Student's t-test $p =$
407 0.65). By contrast, TTX-S current was more than doubled (Figure 5C) in DRG neurons
408 expressing the Y69H variant (-768.21 ± 234.99 pA/pF, $n = 15$), relative to TTX-S current
409 in DRG neurons expressing the wild-type $\beta 2$ subunit (-330.23 ± 66.27 pA/pF, $n = 26$,
410 Student's t-test $p = 0.032$).

411 As DRG neurons express a multiple Na_v channel isoforms, we sought to investigate the
412 Y69H variant in a heterologous system expressing only $\text{Na}_v 1.7$, which is responsible for
413 the majority of TTX-S sodium currents in rat DRG neurons (67). Consistent with our
414 previous results in DRG neurons, we confirmed that the $\beta 2$ -Y69H variant does not alter
415 gating properties (Figure 5D) of $\text{Na}_v 1.7$ channels stably expressed in HEK293 cells.
416 Specifically, the $V_{1/2}$ of activation of $\text{Na}_v 1.7$ in HEK293 cells transfected with the wild-
417 type $\beta 2$ subunit was -22.97 ± 1.58 mV ($n = 16$), which is comparable to those
418 transfected with the Y69H variant (-21.79 ± 1.32 , $n = 20$, Student's t-test $p = 0.57$).
419 Similarly, we did not observe a difference in the $V_{1/2}$ of fast-inactivation of $\text{Nav} 1.7$
420 channels in HEK293 cells transfected with the wild-type $\beta 2$ subunit (-79.60 ± 1.54 mV, n

421 = 17), compared to those transfected with the Y69H variant (-79.73 ± 1.67 mV, $n = 20$,
422 Student's t-test $p = 0.96$). Interestingly, we observed no statistically significant difference
423 in the $\text{Na}_v1.7$ current density (Figure 5E) in these cells, either: current density of $\text{Nav}1.7$
424 in cells transfected with the wild-type $\beta 2$ subunit (-572.67 ± 64.71 pA/pF, $n = 31$) was
425 not different from that in cells transfected with the Y69H variant (-686.57 ± 57.84 pA/pF,
426 $n = 30$, Student's t-test $p = 0.20$).

427

428 **Discussion**

429 While the contribution of β -subunits to sodium channel physiology and neuronal
430 excitability has long been studied, only recently have mutations in β -subunits, and
431 specifically the $\beta 2$ -subunit, been linked to human pain disorders. Here we document the
432 first case of idiopathic small-fiber neuropathy associated with a mutation in the *SCN2B*
433 gene. The expression of the $\beta 2$ -Y69H mutation in small-diameter DRG neurons
434 increases current density of TTX-S channels and renders these neurons hyperexcitable,
435 compared to the wild-type human $\beta 2$ subunit (Figure 6). The expression of the $\beta 2$ -Y69H
436 subunit reduces the threshold to action potential firing, allowing for enhanced repetitive
437 action potential firing. Interestingly, the mechanism underlying this hyperexcitability is a
438 significant increase in TTX-S current density, rather than a major change in channel
439 gating properties. We also report that the co-expression of the $\beta 2$ -Y69H mutant with
440 Nav1.7 channels in HEK293 cells does not recapitulate the increased current density
441 that we observe in DRG neurons, suggesting a cell background-specific mechanism to
442 unmask the effect of this $\beta 2$ subunit mutation.

443 The association of β subunits with the pore-forming α subunits has been shown to
444 regulate channel trafficking to the plasma membrane and gating properties (38). While
445 gain-of-function mutations in α subunits leading to neuropathic pain typically result in
446 biophysical shifts in voltage-dependences of activation or inactivation, or altered
447 recovery from inactivation, changes in channel current density alone are sufficient to
448 alter the excitability of DRG neurons (67); increasing the current density of Nav1.7,
449 which accounts for approximately 70% of TTX-S current density in small-diameter DRG
450 neurons, both reduces the current threshold to action potential firing and enhances

451 repetitive action potential spiking(67). Vasylyev *et al.* used dynamic clamp to precisely
452 modulate the levels of Na_v1.7 current in small-diameter DRG neurons and showed that
453 increasing Na_v1.7 current density by 100% resulted in a near 30% reduction in current
454 threshold. While it would be interesting to compare our results directly to the results
455 from that study, it is not feasible for multiple reasons. Primarily, dynamic clamp injects
456 current using an equation modeling a specific ion channel, but the levels of the physical
457 channel are unchanged. Because we presumably had an increase in the number of
458 TTX-S channels at the cell surface, this may also have affected some change to
459 neuronal excitability, possibly by an interaction with one or more of their many channel
460 binding-partners(68). Additionally, Vasylyev *et al.* only modulated up to a 100% change
461 in Na_v1.7 levels, whereas we recorded an approximately 130% increase in TTX-S
462 current density, so a comparison would both require an extrapolation of their generated
463 fit, as well as an assumption that the Y69H variant increases Na_v1.7 current density
464 exclusively; indeed, we were unable to confirm in a heterologous expression system
465 that the Y69H variant upregulates Na_v1.7 currents. This may imply that the Y69H
466 variant upregulates other TTX-S Na_v channels, such as Na_v1.6, which has also been
467 implicated in pain disorders(69) and shown to regulate sensory neuronal excitability(70).
468 Alternatively, Na_v1.7 may be a target of upregulation by the Y69H variant, but
469 differences in trafficking mechanisms between DRG neurons and HEK293 cells
470 obscured our ability to detect an effect in the latter system. Regardless, it remains clear
471 that the increase in TTX-S current density conferred by the β2-Y69H variant is
472 consistent with neuronal hyperexcitability.

473 Previously, we reported and characterized the first β -subunit mutation, an aspartate-to-
474 asparagine substitution at position 109 in the β 2 subunit, in a patient with a pain
475 syndrome—specifically, diabetic neuropathy(59). Although the D109N variant was
476 discovered in a patient with underlying longstanding diabetes, functional validation of
477 that variant confirmed that it induces neuronal hyperexcitability. Although it is not clear
478 why pain and neuropathy in the patient described here were not manifested until the
479 fifth decade, the discovery of the Y69H β 2 variant, which increased the current density
480 of the TTX-S currents, further strengthens a contributory link between the β 2 subunit
481 and neuropathic pain as no other putative cause of pain was identified.

482 The purported mechanism of action of both the newly identified Y69H variant and the
483 previously identified D109N variant is concordant with established effects of the β 2
484 subunit in DRG neurons. All β -subunits, with the exception of the β 1b splice variant,
485 share the common structure of an extracellular immunoglobulin domain and a
486 transmembrane domain with a short cytoplasmic tail. The Y69H variant is located in the
487 extracellular immunoglobulin domain, which binds to Nav channels within the DII-S5-6
488 extracellular linker via a disulfide bond(39, 71) and enhances channel trafficking to the
489 plasma membrane. This is consistent with the known role of β 2 subunits in small-
490 diameter DRG neurons; Lopez-Santiago *et al.* showed that β 2-null mice DRG neurons
491 exhibited approximately a 50% reduction in TTX-S current and $\text{Na}_v1.7$ protein
492 levels(48).

493 The β 2-Y69H variant was also identified in two patients with Brugada Syndrome, and,
494 when co-expressed with $\text{Na}_v1.5$ in HEK293 cells, resulted in a reduction in current
495 density(72). The data from this early study has only been available in a meeting

496 abstract, and is thus difficult to evaluate. By contrast, the present studies were done in
497 DRG neurons where a full complement of additional factors could be important for
498 uncovering the true effects of this mutation on the TTX-S channels. This data suggests
499 that the Y69H variant may exert its effect in an isoform-specific manner or in a cell
500 background-dependent manner.

501 Both the D109N and Y69H variants are located in the extracellular immunoglobulin
502 domain and both act on TTX-S but not TTX-R channels; however, the mechanism of
503 action for the Y69H variant is distinct from that of the D109N variant. This different
504 mode of action may be influenced by the position of the two residues in the folded
505 structure of the $\beta 2$ subunit. The side chain of the Y69H variant points away from the Nav
506 α subunit (Figure 1), whereas the D109N mutant residue is located in a spatially
507 separate and distinct location within the $\beta 2$ subunit. We postulate that mutations in
508 residues at different loci in the $\beta 2$ subunit may perturb their respective local structures
509 and interfere differentially with normal subunit functioning. For example, based on the
510 data presented in this manuscript, we postulate that mutations facing away from the
511 channel may be more likely to modulate channel trafficking to the cell surface or
512 enhance channel stability at the plasma membrane via interactions with other
513 membrane proteins or extracellular matrix proteins. On the other hand, mutations within
514 local environments closer to the α subunits of TTX-S channels may engage in
515 interactions with the channel itself and cause biophysical alterations in their gating
516 properties. These modes of action of mutations in the $\beta 2$ subunit are difficult to predict
517 using static modeling even with the advances in determining structures of Nav subunits
518 at the atomic level because these structures do not capture the dynamic nature of

519 conformational changes of the channel within the plasma membrane during gating
520 steps.

521 There is a paucity of publications of functional characterization of $\beta 2$ mutations
522 associated with excitability disorders, highlighting the need to fill in this knowledge gap
523 to better understand the contribution of these subunits to normal neuronal physiology
524 and to the effects of mutations of this subunit in the pathophysiology of human pain
525 disorders. The data that we present here, together with our previous publication of a $\beta 2$
526 mutation in a patient with painful diabetic neuropathy(59) strengthens the evidence for a
527 role of these subunits in the pathophysiology of human pain disorders.

528

529 **References**

530 1. **Faber CG, Hoeijmakers JG, Ahn HS, Cheng X, Han C, Choi JS, Estacion M, Lauria G, Vanhoutte**
531 **EK, Gerrits MM, Dib-Hajj S, Drenth JP, Waxman SG, and Merkies IS.** Gain of function Nav1.7 mutations
532 in idiopathic small fiber neuropathy. *Ann Neurol* 71: 26-39, 2012.

533 2. **Sopacua M, Hoeijmakers JGJ, Merkies ISJ, Lauria G, Waxman SG, and Faber CG.** Small-fiber
534 neuropathy: Expanding the clinical pain universe. *J Peripher Nerv Syst* 24: 19-33, 2019.

535 3. **Tesfaye S, Boulton AJ, Dyck PJ, Freeman R, Horowitz M, Kempler P, Lauria G, Malik RA,**
536 **Spallone V, Vinik A, Bernardi L, and Valensi P.** Diabetic neuropathies: update on definitions, diagnostic
537 criteria, estimation of severity, and treatments. *Diabetes Care* 33: 2285-2293, 2010.

538 4. **Han Y, and Smith MT.** Pathobiology of cancer chemotherapy-induced peripheral neuropathy
539 (CIPN). *Front Pharmacol* 4: 156, 2013.

540 5. **Devigili G, Rinaldo S, Lombardi R, Cazzato D, Marchi M, Salvi E, Eleopra R, and Lauria G.**
541 Diagnostic criteria for small fibre neuropathy in clinical practice and research. *Brain* 142: 3728-3736,
542 2019.

543 6. **Bakkers M, Faber CG, Hoeijmakers JG, Lauria G, and Merkies IS.** Small fibers, large impact:
544 quality of life in small-fiber neuropathy. *Muscle Nerve* 49: 329-336, 2014.

545 7. **Schaefer C, Mann R, Sadosky A, Daniel S, Parsons B, Nalamachu S, Stacey BR, Tuchman M,**
546 **Anschel A, and Nieshoff E.** Health status, function, productivity, and costs among individuals with
547 idiopathic painful peripheral neuropathy with small fiber involvement in the United States: results from
548 a retrospective chart review and cross-sectional survey. *J Med Econ* 17: 394-407, 2014.

549 8. **Nishikawa N, and Nomoto M.** Management of neuropathic pain. *J Gen Fam Med* 18: 56-60,
550 2017.

551 9. **Finnerup NB, Attal N, Haroutounian S, McNicol E, Baron R, Dworkin RH, Gilron I, Haanpaa M,**
552 **Hansson P, Jensen TS, Kamerman PR, Lund K, Moore A, Raja SN, Rice AS, Rowbotham M, Sena E,**
553 **Siddall P, Smith BH, and Wallace M.** Pharmacotherapy for neuropathic pain in adults: a systematic
554 review and meta-analysis. *Lancet Neurol* 14: 162-173, 2015.

555 10. **de Greef BTA, Hoeijmakers JGJ, Gorissen-Brouwers CML, Geerts M, Faber CG, and Merkies ISJ.**
556 Associated conditions in small fiber neuropathy - a large cohort study and review of the literature. *Eur J*
557 *Neurol* 25: 348-355, 2018.

558 11. **Brouwer BA, Merkies IS, Gerrits MM, Waxman SG, Hoeijmakers JG, and Faber CG.** Painful
559 neuropathies: the emerging role of sodium channelopathies. *J Peripher Nerv Syst* 19: 53-65, 2014.

560 12. **Lehmann HC, Wunderlich G, Fink GR, and Sommer C.** Diagnosis of peripheral neuropathy.
561 *Neurol Res Pract* 2: 20, 2020.

562 13. **Huang J, Yang Y, Zhao P, Gerrits MM, Hoeijmakers JG, Bekelaar K, Merkies IS, Faber CG, Dib-**
563 **Hajj SD, and Waxman SG.** Small-Fiber Neuropathy Nav1.8 Mutation Shifts Activation to Hyperpolarized
564 Potentials and Increases Excitability of Dorsal Root Ganglion Neurons. *J Neurosci* 33: 14087-14097, 2013.

565 14. **Faber CG, Lauria G, Merkies IS, Cheng X, Han C, Ahn HS, Persson AK, Hoeijmakers JG, Gerrits**
566 **MM, Pierro T, Lombardi R, Kapetis D, Dib-Hajj SD, and Waxman SG.** Gain-of-function Nav1.8 mutations
567 in painful neuropathy. *Proc Natl Acad Sci U S A* 109: 19444-19449, 2012b.

568 15. **Huang J, Han C, Estacion M, Vasylyev D, Hoeijmakers JG, Gerrits MM, Tyrrell L, Lauria G, Faber**
569 **CG, Dib-Hajj SD, Merkies IS, Waxman SG, and Group PS.** Gain-of-function mutations in sodium channel
570 Na(v)1.9 in painful neuropathy. *Brain* 137: 1627-1642, 2014.

571 16. **Eijkenboom I, Sopacua M, Hoeijmakers JGJ, de Greef BTA, Lindsey P, Almomani R, Marchi M,**
572 **Vanoevelen J, Smeets HJM, Waxman SG, Lauria G, Merkies ISJ, Faber CG, and Gerrits MM.** Yield of
573 peripheral sodium channels gene screening in pure small fibre neuropathy. *J Neurol Neurosurg*
574 *Psychiatry* 90: 342-352, 2019.

- 575 17. **Vlckova-Moravcova E, Bednarik J, Belobradkova J, and Sommer C.** Small-fibre involvement in
576 diabetic patients with neuropathic foot pain. *Diabet Med* 25: 692-699, 2008.
- 577 18. **Brewer JR, Morrison G, Dolan ME, and Fleming GF.** Chemotherapy-induced peripheral
578 neuropathy: Current status and progress. *Gynecol Oncol* 140: 176-183, 2016.
- 579 19. **Bednarik J, Vlckova-Moravcova E, Bursova S, Belobradkova J, Dusek L, and Sommer C.** Etiology
580 of small-fiber neuropathy. *J Peripher Nerv Syst* 14: 177-183, 2009.
- 581 20. **de Greef BTA, Hoeijmakers JGJ, Geerts M, Oakes M, Church TJE, Waxman SG, Dib-Hajj SD,
582 Faber CG, and Merkies ISJ.** Lacosamide in patients with Nav1.7 mutations-related small fibre
583 neuropathy: a randomized controlled trial. *Brain* 142: 263-275, 2019.
- 584 21. **Waxman SG.** The neuron as a dynamic electrogenic machine: modulation of sodium-channel
585 expression as a basis for functional plasticity in neurons. *Philos Trans R Soc Lond B Biol Sci* 355: 199-213,
586 2000.
- 587 22. **Hodgkin AL, and Huxley AF.** A quantitative description of membrane current and its application
588 to conduction and excitation in nerve. *J Physiol* 117: 500-544, 1952.
- 589 23. **Catterall WA, Llenaues MJ, and Gamal El-Din TM.** Structure and Pharmacology of Voltage-Gated
590 Sodium and Calcium Channels. *Annu Rev Pharmacol Toxicol* 60: 133-154, 2020.
- 591 24. **Yu FH, and Catterall WA.** Overview of the voltage-gated sodium channel family. *Genome Biol* 4:
592 207, 2003.
- 593 25. **Dib-Hajj SD, Yang Y, Black JA, and Waxman SG.** The Na(V)1.7 sodium channel: from molecule to
594 man. *Nat Rev Neurosci* 14: 49-62, 2013.
- 595 26. **Han C, Huang J, and Waxman SG.** Sodium channel Nav1.8: Emerging links to human disease.
596 *Neurology* 86: 473-483, 2016.
- 597 27. **Bennett DL, Clark AJ, Huang J, Waxman SG, and Dib-Hajj SD.** The Role of Voltage-Gated Sodium
598 Channels in Pain Signaling. *Physiol Rev* 99: 1079-1151, 2019.
- 599 28. **Yang Y, Wang Y, Li S, Xu Z, Li H, Ma L, Fan J, Bu D, Liu B, Fan Z, Wu G, Jin J, Ding B, Zhu X, and
600 Shen Y.** Mutations in SCN9A, encoding a sodium channel alpha subunit, in patients with primary
601 erythromelgia. *J Med Genet* 41: 171-174, 2004.
- 602 29. **Cummins TR, Dib-Hajj SD, and Waxman SG.** Electrophysiological properties of mutant Nav1.7
603 sodium channels in a painful inherited neuropathy. *J Neurosci* 24: 8232-8236, 2004.
- 604 30. **Dib-Hajj SD, Rush AM, Cummins TR, Hisama FM, Novella S, Tyrrell L, Marshall L, and Waxman
605 SG.** Gain-of-function mutation in Nav1.7 in familial erythromelgia induces bursting of sensory neurons.
606 *Brain* 128: 1847-1854, 2005.
- 607 31. **Han C, Rush AM, Dib-Hajj SD, Li S, Xu Z, Wang Y, Tyrrell L, Wang X, Yang Y, and Waxman SG.**
608 Sporadic onset of erythromelgia: a gain-of-function mutation in Nav1.7. *Ann Neurol* 59: 553-558, 2006.
- 609 32. **Lampert A, Dib-Hajj SD, Tyrrell L, and Waxman SG.** Size matters: Erythromelgia mutation
610 S241T in Nav1.7 alters channel gating. *J Biol Chem* 281: 36029-36035, 2006.
- 611 33. **Cox JJ, Reimann F, Nicholas AK, Thornton G, Roberts E, Springell K, Karbani G, Jafri H, Mannan
612 J, Raashid Y, Al-Gazali L, Hamamy H, Valente EM, Gorman S, Williams R, McHale DP, Wood JN, Gribble
613 FM, and Woods CG.** An SCN9A channelopathy causes congenital inability to experience pain. *Nature*
614 444: 894-898, 2006.
- 615 34. **Goldberg YP, MacFarlane J, MacDonald ML, Thompson J, Dube MP, Mattice M, Fraser R,
616 Young C, Hossain S, Pape T, Payne B, Radomski C, Donaldson G, Ives E, Cox J, Younghusband HB, Green
617 R, Duff A, Boltshauser E, Grinspan GA, Dimon JH, Sibley BG, Andria G, Toscano E, Kerdraon J, Bowsher
618 D, Pimstone SN, Samuels ME, Sherrington R, and Hayden MR.** Loss-of-function mutations in the Nav1.7
619 gene underlie congenital indifference to pain in multiple human populations. *Clin Genet* 71: 311-319,
620 2007.

- 621 35. **Ahmad S, Dahllund L, Eriksson AB, Hellgren D, Karlsson U, Lund PE, Meijer IA, Meury L, Mills T,**
622 **Moody A, Morinville A, Morten J, O'Donnell D, Raynoschek C, Salter H, Rouleau GA, and Krupp JJ.** A
623 stop codon mutation in SCN9A causes lack of pain sensation. *Hum Mol Genet* 16: 2114-2121, 2007.
- 624 36. **Han C, Vasylyev D, Macala LJ, Gerrits MM, Hoeijmakers JG, Bekelaar KJ, Dib-Hajj SD, Faber CG,**
625 **Merkies IS, and Waxman SG.** The G1662S Nav1.8 mutation in small fibre neuropathy: impaired
626 inactivation underlying DRG neuron hyperexcitability. *J Neurol Neurosurg Psychiatry* 85: 499-505, 2014.
- 627 37. **Chahine M, and O'Leary ME.** Regulatory Role of Voltage-Gated Na Channel beta Subunits in
628 Sensory Neurons. *Front Pharmacol* 2: 70, 2011.
- 629 38. **Bouza AA, and Isom LL.** Voltage-Gated Sodium Channel β Subunits and Their Related Diseases.
630 *Handb Exp Pharmacol* 246: 423-450, 2018.
- 631 39. **Shen H, Liu D, Wu K, Lei J, and Yan N.** Structures of human Na(v)1.7 channel in complex with
632 auxiliary subunits and animal toxins. *Science* 363: 1303-1308, 2019.
- 633 40. **Mantegazza M, and Catterall WA.** Voltage-Gated Na(+) Channels: Structure, Function, and
634 Pathophysiology. In: *Jasper's Basic Mechanisms of the Epilepsies*, edited by Noebels JL, Avoli M,
635 Rogawski MA, Olsen RW, and Delgado-Escueta AV. Bethesda MD: © 2012, Michael A Rogawski, Antonio
636 V Delgado-Escueta, Jeffrey L Noebels, Massimo Avoli and Richard W Olsen., 2012.
- 637 41. **Sokolov MV, Henrich-Noack P, Raynoschek C, Franzén B, Larsson O, Main M, and Dabrowski**
638 **M.** Co-expression of β Subunits with the Voltage-Gated Sodium Channel Na(V)1.7: the Importance of
639 Subunit Association and Phosphorylation and Their Effects on Channel Pharmacology and Biophysics. *J*
640 *Mol Neurosci* 65: 154-166, 2018.
- 641 42. **Cusdin FS, Nietlispach D, Maman J, Dale TJ, Powell AJ, Clare JJ, and Jackson AP.** The sodium
642 channel {beta}3-subunit induces multiphasic gating in Nav1.3 and affects fast inactivation via distinct
643 intracellular regions. *J Biol Chem* 285: 33404-33412, 2010.
- 644 43. **Johnson D, Montpetit ML, Stocker PJ, and Bennett ES.** The sialic acid component of the beta1
645 subunit modulates voltage-gated sodium channel function. *J Biol Chem* 279: 44303-44310, 2004.
- 646 44. **Isom LL, De Jongh KS, Patton DE, Reber BF, Offord J, Charbonneau H, Walsh K, Goldin AL, and**
647 **Catterall WA.** Primary structure and functional expression of the beta 1 subunit of the rat brain sodium
648 channel. *Science* 256: 839-842, 1992.
- 649 45. **Brackenbury WJ, Calhoun JD, Chen C, Miyazaki H, Nukina N, Oyama F, Ranscht B, and Isom LL.**
650 Functional reciprocity between Na⁺ channel Nav1.6 and beta1 subunits in the coordinated regulation of
651 excitability and neurite outgrowth. *Proc Natl Acad Sci U S A* 107: 2283-2288, 2010.
- 652 46. **Laedermann CJ, Syam N, Pertin M, Decosterd I, and Abriel H.** β 1- and β 3- voltage-gated sodium
653 channel subunits modulate cell surface expression and glycosylation of Nav1.7 in HEK293 cells. *Front Cell*
654 *Neurosci* 7: 137, 2013.
- 655 47. **Cummins TR, Aglietto F, Renganathan M, Herzog RI, Dib-Hajj SD, and Waxman SG.** Nav1.3
656 sodium channels: rapid repriming and slow closed-state inactivation display quantitative differences
657 after expression in a mammalian cell line and in spinal sensory neurons. *J Neurosci* 21: 5952-5961, 2001.
- 658 48. **Lopez-Santiago LF, Pertin M, Morisod X, Chen C, Hong S, Wiley J, Decosterd I, and Isom LL.**
659 Sodium channel beta2 subunits regulate tetrodotoxin-sensitive sodium channels in small dorsal root
660 ganglion neurons and modulate the response to pain. *J Neurosci* 26: 7984-7994, 2006.
- 661 49. **Chen C, Bharucha V, Chen Y, Westenbroek RE, Brown A, Malhotra JD, Jones D, Avery C,**
662 **Gillespie PJ, 3rd, Kazen-Gillespie KA, Kazarinova-Noyes K, Shrager P, Saunders TL, Macdonald RL,**
663 **Ransom BR, Scheuer T, Catterall WA, and Isom LL.** Reduced sodium channel density, altered voltage
664 dependence of inactivation, and increased susceptibility to seizures in mice lacking sodium channel beta
665 2-subunits. *Proc Natl Acad Sci U S A* 99: 17072-17077, 2002.
- 666 50. **Shimizu H, Tosaki A, Ohsawa N, Ishizuka-Katsura Y, Shoji S, Miyazaki H, Oyama F, Terada T,**
667 **Shirouzu M, Sekine SI, Nukina N, and Yokoyama S.** Parallel homodimer structures of the extracellular

668 domains of the voltage-gated sodium channel beta4 subunit explain its role in cell-cell adhesion. *J Biol*
669 *Chem* 292: 13428-13440, 2017.

670 51. **Xiong H, Yang Q, Zhang X, Wang P, Chen F, Liu Y, Wang P, Zhao Y, Li S, Huang Y, Chen S, Wang**
671 **X, Zhang H, Yu D, Tan C, Fang C, Huang Y, Wu G, Wu Y, Cheng X, Liao Y, Zhang R, Yang Y, Ke T, Ren X, Li**
672 **H, Tu X, Xia Y, Xu C, Chen Q, and Wang QK.** Significant association of rare variant p.Gly8Ser in cardiac
673 sodium channel β 4-subunit SCN4B with atrial fibrillation. *Ann Hum Genet* 83: 239-248, 2019.

674 52. **Riuró H, Beltran-Alvarez P, Tarradas A, Selga E, Campuzano O, Vergés M, Pagans S, Iglesias A,**
675 **Brugada J, Brugada P, Vázquez FM, Pérez GJ, Scornik FS, and Brugada R.** A missense mutation in the
676 sodium channel β 2 subunit reveals SCN2B as a new candidate gene for Brugada syndrome. *Hum Mutat*
677 34: 961-966, 2013.

678 53. **Wallace RH, Wang DW, Singh R, Scheffer IE, George AL, Jr., Phillips HA, Saar K, Reis A, Johnson**
679 **EW, Sutherland GR, Berkovic SF, and Mulley JC.** Febrile seizures and generalized epilepsy associated
680 with a mutation in the Na⁺-channel beta1 subunit gene SCN1B. *Nat Genet* 19: 366-370, 1998.

681 54. **Meadows LS, Malhotra J, Loukas A, Thyagarajan V, Kazen-Gillespie KA, Koopman MC, Kriegler**
682 **S, Isom LL, and Ragsdale DS.** Functional and biochemical analysis of a sodium channel beta1 subunit
683 mutation responsible for generalized epilepsy with febrile seizures plus type 1. *J Neurosci* 22: 10699-
684 10709, 2002.

685 55. **Audenaert D, Claes L, Ceulemans B, Löfgren A, Van Broeckhoven C, and De Jonghe P.** A
686 deletion in SCN1B is associated with febrile seizures and early-onset absence epilepsy. *Neurology* 61:
687 854-856, 2003.

688 56. **Patino GA, Claes LR, Lopez-Santiago LF, Slat EA, Dondeti RS, Chen C, O'Malley HA, Gray CB,**
689 **Miyazaki H, Nukina N, Oyama F, De Jonghe P, and Isom LL.** A functional null mutation of SCN1B in a
690 patient with Dravet syndrome. *J Neurosci* 29: 10764-10778, 2009.

691 57. **Pertin M, Ji RR, Berta T, Powell AJ, Karchewski L, Tate SN, Isom LL, Woolf CJ, Gilliard N, Spahn**
692 **DR, and Decosterd I.** Upregulation of the voltage-gated sodium channel beta2 subunit in neuropathic
693 pain models: characterization of expression in injured and non-injured primary sensory neurons. *J*
694 *Neurosci* 25: 10970-10980, 2005.

695 58. **Xie W, Zhang J, Strong JA, and Zhang JM.** Role of Na(V)1.6 and Na(V) β 4 Sodium Channel
696 Subunits in a Rat Model of Low Back Pain Induced by Compression of the Dorsal Root Ganglia.
697 *Neuroscience* 402: 51-65, 2019.

698 59. **Alsalam M, Estacion M, Almomani R, Gerrits MM, Bönhof GJ, Ziegler D, Malik R, Ferdousi M,**
699 **Lauria G, Merkies IS, Faber CG, Dib-Hajj S, and Waxman SG.** A gain-of-function sodium channel β 2-
700 subunit mutation in painful diabetic neuropathy. *Mol Pain* 15: 1744806919849802, 2019.

701 60. **Almomani R, Marchi M, Sopacua M, Lindsey P, Salvi E, Koning B, Santoro S, Magri S, Smeets**
702 **HJM, Martinelli Boneschi F, Malik RR, Ziegler D, Hoeijmakers JGJ, Bonhof G, Dib-Hajj S, Waxman SG,**
703 **Merkies ISJ, Lauria G, Faber CG, Gerrits MM, and on behalf on the PSG.** Evaluation of molecular
704 inversion probe versus TruSeq(R) custom methods for targeted next-generation sequencing. *PLoS One*
705 15: e0238467, 2020.

706 61. **Lossin C, Wang DW, Rhodes TH, Vanoye CG, and George AL, Jr.** Molecular basis of an inherited
707 epilepsy. *Neuron* 34: 877-884, 2002.

708 62. **Dib-Hajj SD, Choi JS, Macala LJ, Tyrrell L, Black JA, Cummins TR, and Waxman SG.** Transfection
709 of rat or mouse neurons by biolistics or electroporation. *Nat Protoc* 4: 1118-1126, 2009.

710 63. **Jo S, Kim T, Iyer VG, and Im W.** CHARMM-GUI: a web-based graphical user interface for
711 CHARMM. *J Comput Chem* 29: 1859-1865, 2008.

712 64. **Karczewski KJ, Francioli LC, Tiao G, Cummings BB, Alföldi J, Wang Q, Collins RL, Laricchia KM,**
713 **Ganna A, Birnbaum DP, Gauthier LD, Brand H, Solomonson M, Watts NA, Rhodes D, Singer-Berk M,**
714 **England EM, Seaby EG, Kosmicki JA, Walters RK, Tashman K, Farjoun Y, Banks E, Poterba T, Wang A,**
715 **Seed C, Whiffin N, Chong JX, Samocha KE, Pierce-Hoffman E, Zappala Z, O'Donnell-Luria AH, Minikel**

716 EV, Weisburd B, Lek M, Ware JS, Vittal C, Armean IM, Bergelson L, Cibulskis K, Connolly KM,
717 Covarrubias M, Donnelly S, Ferriera S, Gabriel S, Gentry J, Gupta N, Jeandet T, Kaplan D, Llanwarne C,
718 Munshi R, Novod S, Petrillo N, Roazen D, Ruano-Rubio V, Saltzman A, Schleicher M, Soto J, Tibbetts K,
719 Tolonen C, Wade G, Talkowski ME, Aguilar Salinas CA, Ahmad T, Albert CM, Ardissino D, Atzmon G,
720 Barnard J, Beaugerie L, Benjamin EJ, Boehnke M, Bonnycastle LL, Bottinger EP, Bowden DW, Bown MJ,
721 Chambers JC, Chan JC, Chasman D, Cho J, Chung MK, Cohen B, Correa A, Dabelea D, Daly MJ, Darbar D,
722 Duggirala R, Dupuis J, Ellinor PT, Elosua R, Erdmann J, Esko T, Färkkilä M, Florez J, Franke A, Getz G,
723 Glaser B, Glatt SJ, Goldstein D, Gonzalez C, Groop L, Haiman C, Hanis C, Harms M, Hiltunen M, Holi
724 MM, Hultman CM, Kallela M, Kaprio J, Kathiresan S, Kim B-J, Kim YJ, Kirov G, Kooner J, Koskinen S,
725 Krumholz HM, Kugathasan S, Kwak SH, Laakso M, Lehtimäki T, Loos RJF, Lubitz SA, Ma RCW,
726 MacArthur DG, Marrugat J, Mattila KM, McCarroll S, McCarthy MI, McGovern D, McPherson R, Meigs
727 JB, Melander O, Metspalu A, Neale BM, Nilsson PM, O'Donovan MC, Ongur D, Orozco L, Owen MJ,
728 Palmer CNA, Palotie A, Park KS, Pato C, Pulver AE, Rahman N, Remes AM, Rioux JD, Ripatti S, Roden
729 DM, Saleheen D, Salomaa V, Samani NJ, Scharf J, Schunkert H, Shoemaker MB, Sklar P, Soininen H,
730 Sokol H, Spector T, Sullivan PF, Suvisaari J, Tai ES, Teo YY, Tiinamaija T, Tsuang M, Turner D, Tusie-Luna
731 T, Vartiainen E, Ware JS, Watkins H, Weersma RK, Wessman M, Wilson JG, Xavier RJ, Neale BM, Daly
732 MJ, MacArthur DG, and Genome Aggregation Database C. The mutational constraint spectrum
733 quantified from variation in 141,456 humans. *Nature* 581: 434-443, 2020.

734 65. Olesen MS, Andreassen L, Jabbari J, Refsgaard L, Haunsø S, Olesen SP, Nielsen JB, Schmitt N,
735 and Svendsen JH. Very early-onset lone atrial fibrillation patients have a high prevalence of rare variants
736 in genes previously associated with atrial fibrillation. *Heart Rhythm* 11: 246-251, 2014.

737 66. Isom LL, Ragsdale DS, De Jongh KS, Westenbroek RE, Reber BF, Scheuer T, and Catterall WA.
738 Structure and function of the beta 2 subunit of brain sodium channels, a transmembrane glycoprotein
739 with a CAM motif. *Cell* 83: 433-442, 1995.

740 67. Vasylyev DV, Han C, Zhao P, Dib-Hajj S, and Waxman SG. Dynamic-clamp analysis of wild-type
741 human Nav1.7 and erythromelalgia mutant channel L858H. *J Neurophysiol* 111: 1429-1443, 2014.

742 68. Kanellopoulos AH, Koenig J, Huang H, Pyrski M, Millet Q, Lolignier S, Morohashi T, Gossage SJ,
743 Jay M, Linley JE, Baskozos G, Kessler BM, Cox JJ, Dolphin AC, Zufall F, Wood JN, and Zhao J. Mapping
744 protein interactions of sodium channel NaV1.7 using epitope-tagged gene-targeted mice. *EMBO J* 37:
745 427-445, 2018.

746 69. Tanaka BS, Zhao P, Dib-Hajj FB, Morisset V, Tate S, Waxman SG, and Dib-Hajj SD. A gain-of-
747 function mutation in Nav1.6 in a case of trigeminal neuralgia. *Mol Med* 22: 338-348, 2016.

748 70. Israel MR, Tanaka BS, Castro J, Thongyoo P, Robinson SD, Zhao P, Deuis JR, Craik DJ, Durek T,
749 Brierley SM, Waxman SG, Dib-Hajj SD, and Vetter I. Na(V) 1.6 regulates excitability of mechanosensitive
750 sensory neurons. *J Physiol* 597: 3751-3768, 2019.

751 71. Chen C, Calhoun JD, Zhang Y, Lopez-Santiago L, Zhou N, Davis TH, Salzer JL, and Isom LL.
752 Identification of the Cysteine Residue Responsible for Disulfide Linkage of Na⁺ Channel α and β 2
753 Subunits*. *Journal of Biological Chemistry* 287: 39061-39069, 2012.

754 72. Hu D, Barajas-Martinez H, Medeiros-Domingo A, Crotti L, Tester D, Veltmann C, Schimpf R,
755 Pfeiffer R, Dezi F, Liu Y, Burashnikov E, Guidicessi JR, Ye D, Wolpert C, Borggrefe M, Schwartz P,
756 Ackerman MJ, and Antzelevitch C. Abstract 16521: Novel Mutations in the Sodium Channel 2 Subunit
757 Gene (SCN2B) Associated with Brugada Syndrome and Atrial Fibrillation. *Circulation* 126: A16521, 2012.

758

759

760

761 **Table 1.** Fast-inactivation properties in DRG neurons expressing either the wild-type or
 762 Y69H $\beta 2$ subunit.

	Wild-type (n = 14)	Y69H (n = 12)	Student's t-test p-value
TTX-R $V_{1/2}$	-45.10 \pm 1.81	-43.61 \pm 2.14	0.60
TTX-R slope	6.18 \pm 0.32	6.035 \pm 0.83	0.86
TTX-S $V_{1/2}$	-75.48 \pm 1.76	-79.22 \pm 1.87	0.16
TTX-S slope	5.31 \pm 0.59	5.89 \pm 0.78	0.55

763

764 **Figure Legends**

765 **Figure 1.** Molecular modeling of the $\beta 2$ -Y69H variant. The immunoglobulin domain of
 766 the human $\beta 2$ subunit (cyan) is linked to the $Na_v 1.7$ channel α subunit (green) via a
 767 disulfide bond with the cysteine at position 55 (C55, yellow). The sidechain of the tyrosine
 768 at position 69 (Y69, magenta) is shown, facing away from the α subunit. The star in the
 769 cartoon diagram of the $\beta 2$ subunit (top right) indicates the relative position of the
 770 mutation. The sidechain of the aspartic acid at position 109 (D109, orange) is also
 771 shown. The α subunit is embedded in a lipid bilayer membrane (red, white, and green
 772 spheres). A small portion of the $\beta 1$ subunit (red, top left) may be seen, as well.

773 **Figure 2.** The Y69H variant does not alter resting membrane potential of DRG neurons.
 774 **(A)** Comparison of resting membrane potentials for DRG neurons expressing either the
 775 wild-type human $\beta 2$ subunit (monochrome) or the Y69H variant (orange) illustrates no
 776 change in neuronal RMP. **(B)** A numerically larger, but not statistically significant,
 777 proportion of DRG neurons expressing the Y69H variant fire spontaneous action
 778 potentials at rest than DRG neurons expressing the wild-type human $\beta 2$ subunit.

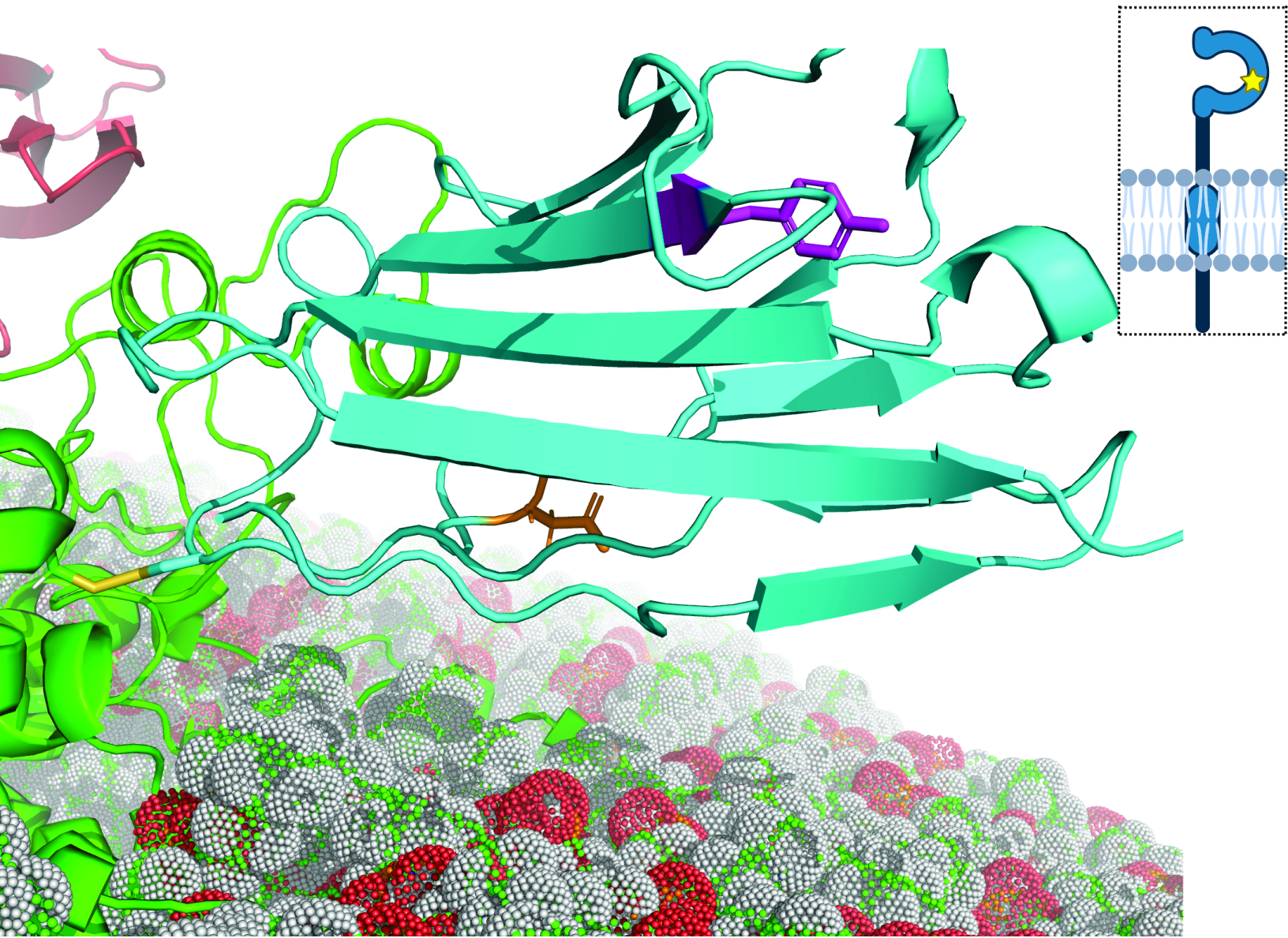
779 **Figure 3.** The Y69H variant reduces the threshold of action potential firing and
 780 enhances repetitive spiking in DRG neurons. **(A)** Representative traces depicting the
 781 action potential response of DRG neurons expressing the wild-type (black) or Y69H

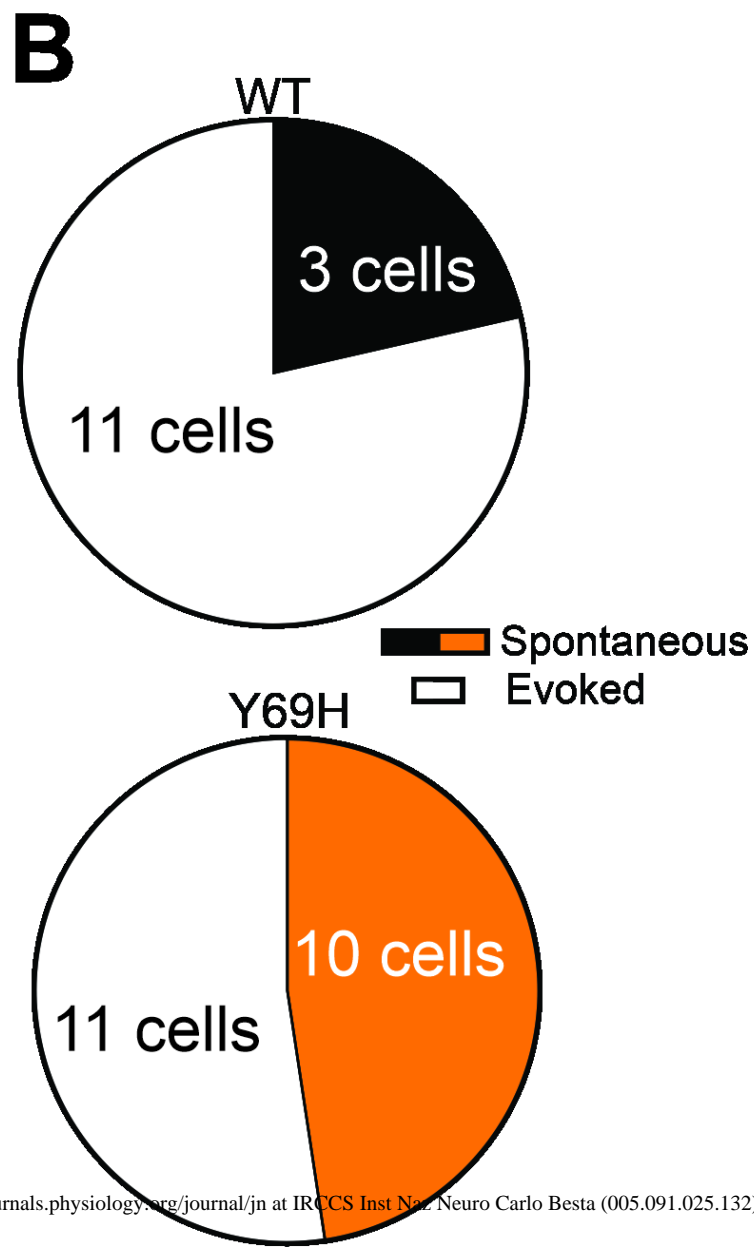
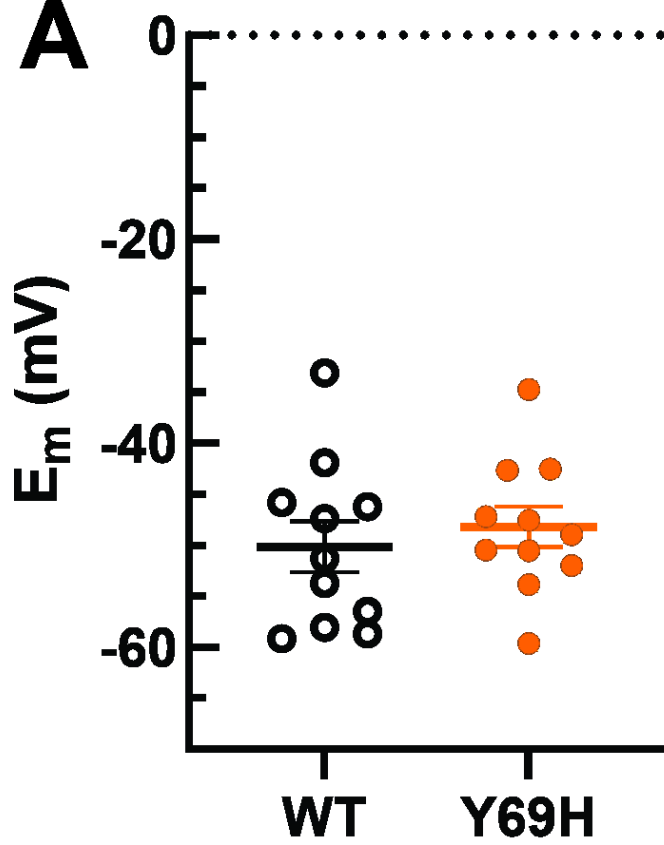
782 variant (orange) human $\beta 2$ subunit during stimulation with current injections of 200 ms
783 duration. The 0 mV membrane potential is indicated by the dashed line. **(B)** DRG
784 neurons expressing the Y69H variant displayed a significantly lower threshold to action
785 potential firing than did neurons expressing the wild-type $\beta 2$ subunit. **(C)** When neurons
786 were stimulated with a 1000 ms pulse at the threshold amplitude as determined by a
787 200 ms injection in **(B)**, DRG neurons expressing the Y69H variant fired significantly
788 more action potentials than those expressing the wild-type $\beta 2$ subunit. **(D)**
789 Representative traces depicting repetitive action potential firing of DRG neurons
790 expressing the Y69H variant (orange), compared to those expressing the wild-type $\beta 2$
791 subunit (black). **(E)** Neurons expressing the Y69H variant (orange) fired significantly
792 more action potentials during a 1000 ms stimulus of graded amplitude than did neurons
793 expressing the wild-type $\beta 2$ subunit (monochrome).

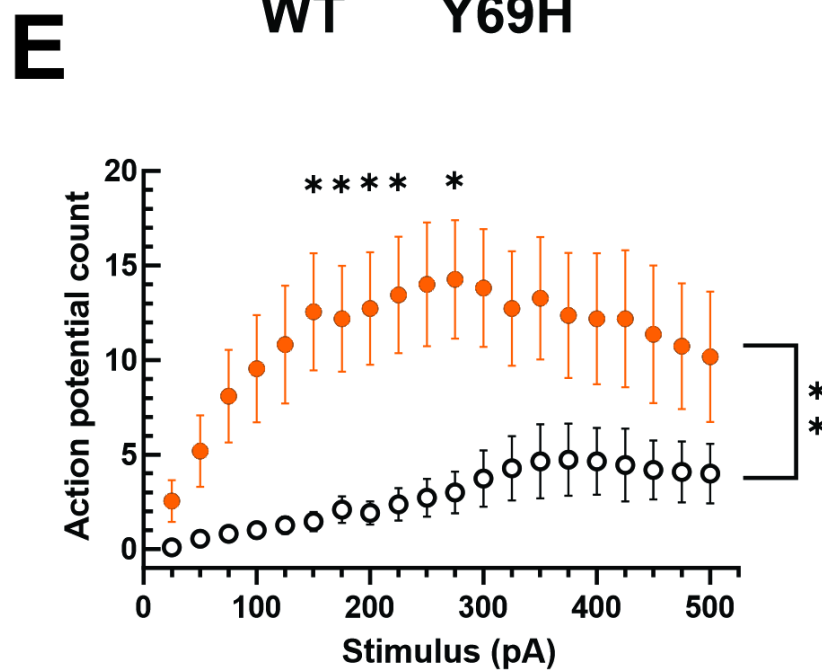
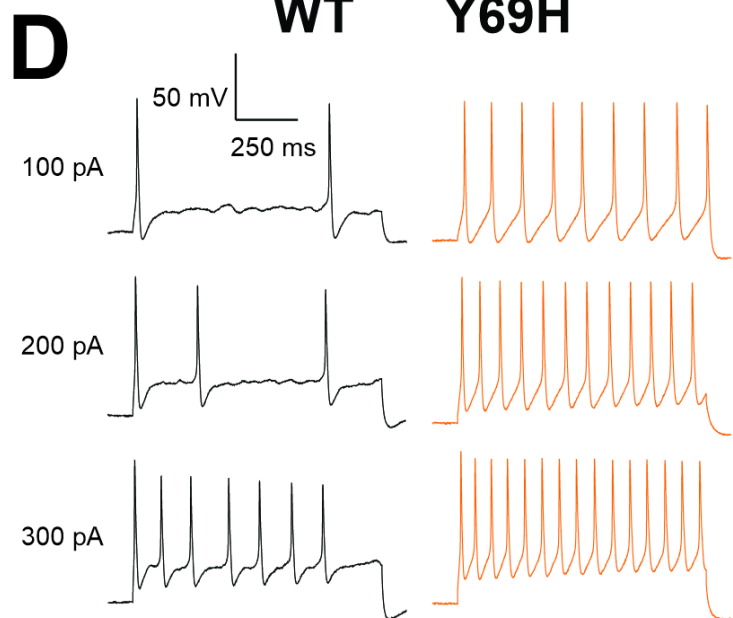
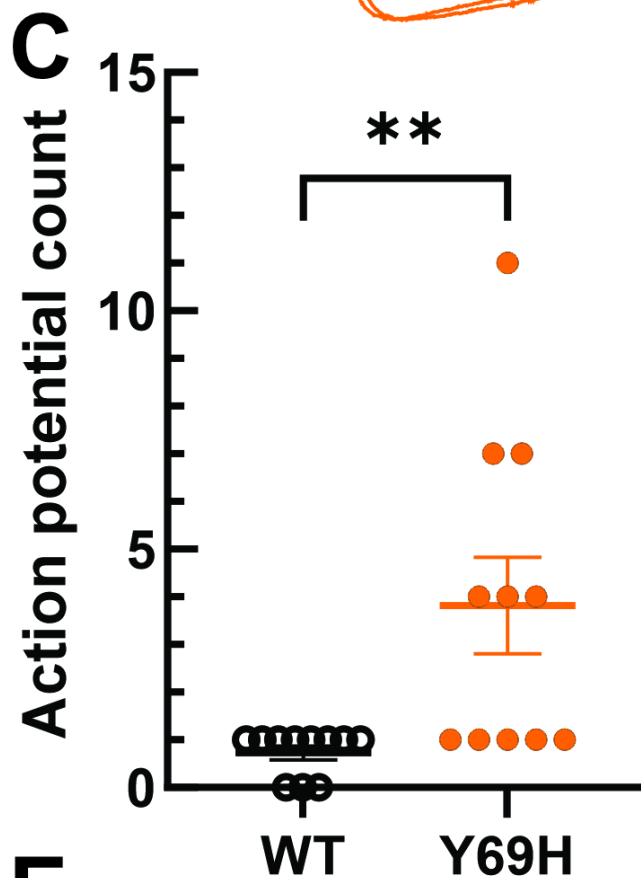
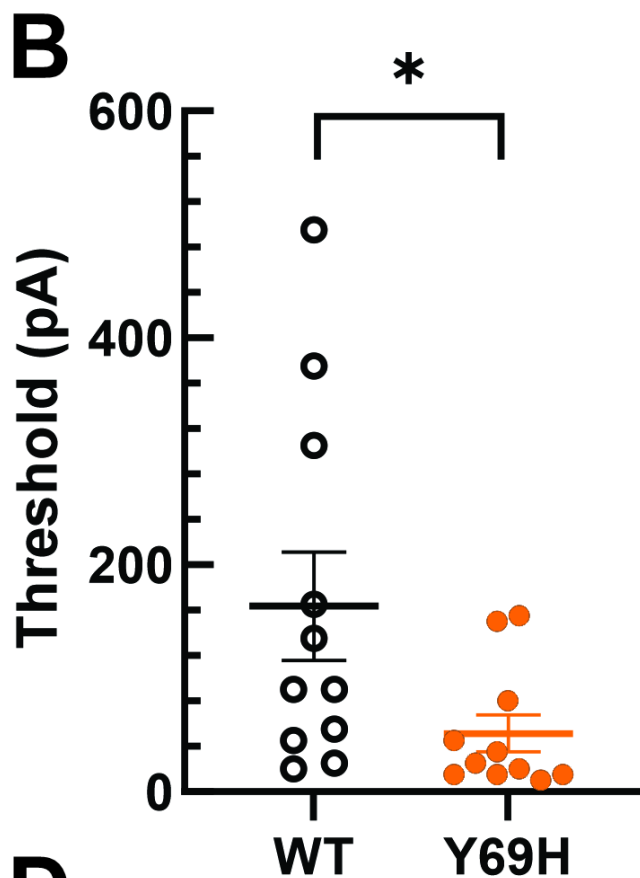
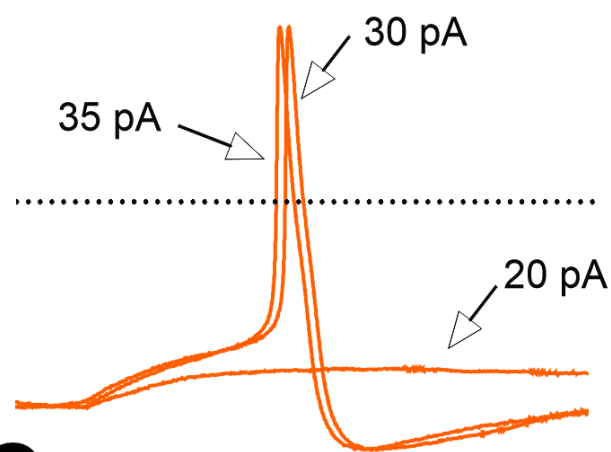
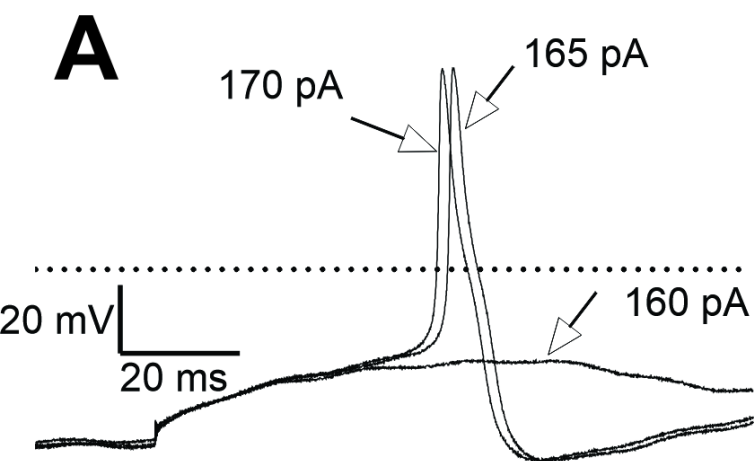
794 **Figure 4.** The Y69H variant does not alter total Na_v channel gating properties. **(A)** The
795 voltage-dependence of channel inactivation (left; diamonds) are not statistically different
796 between DRG neurons expressing the wild-type and Y69H variant subunits.
797 Additionally, the voltage-dependence of activation (right, circles) is also not statistically
798 different. **(B)** There is no difference in the use-dependent inhibition of sodium channels
799 in DRG neurons expressing either the wild-type or the Y69H $\beta 2$ subunit. **(C)** The extent
800 of sodium channel recovery from inactivation at voltages between -70 and -120 mV is
801 comparable for DRG neurons expressing either the wild-type or the variant $\beta 2$ subunits.
802 **(D)** The rate of recovery from channel inactivation is also comparable in both groups.
803 **(E)** There is no difference in the kinetics of entry into deactivation between DRG
804 neurons expressing the wild-type or Y69H variant.

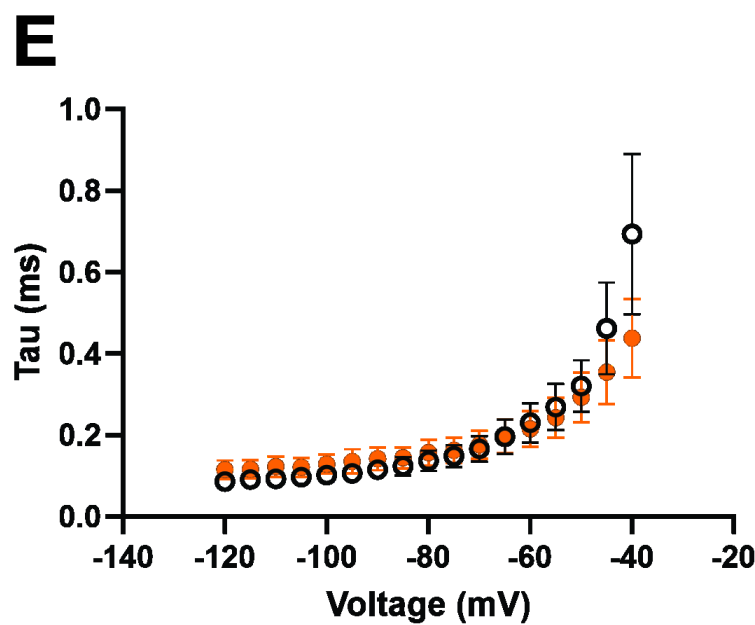
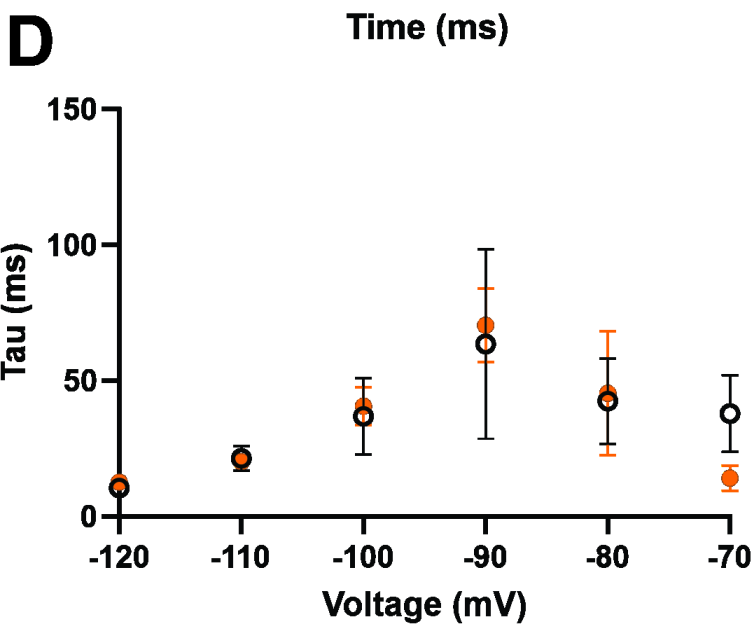
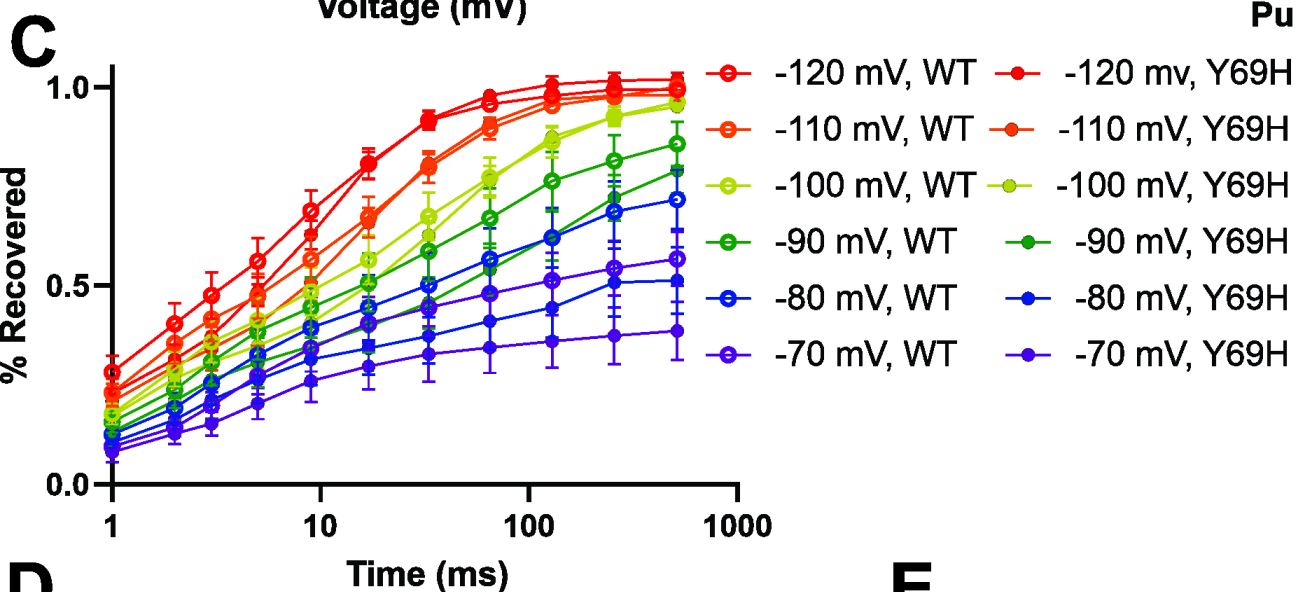
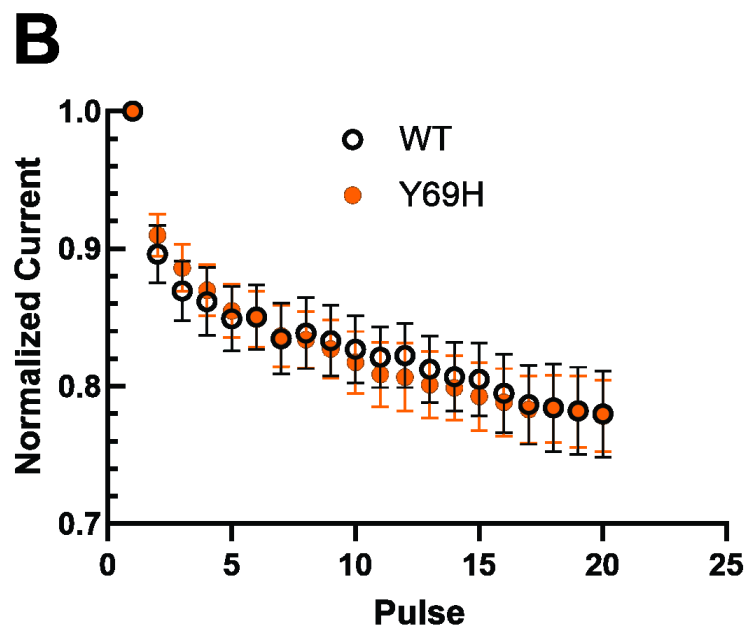
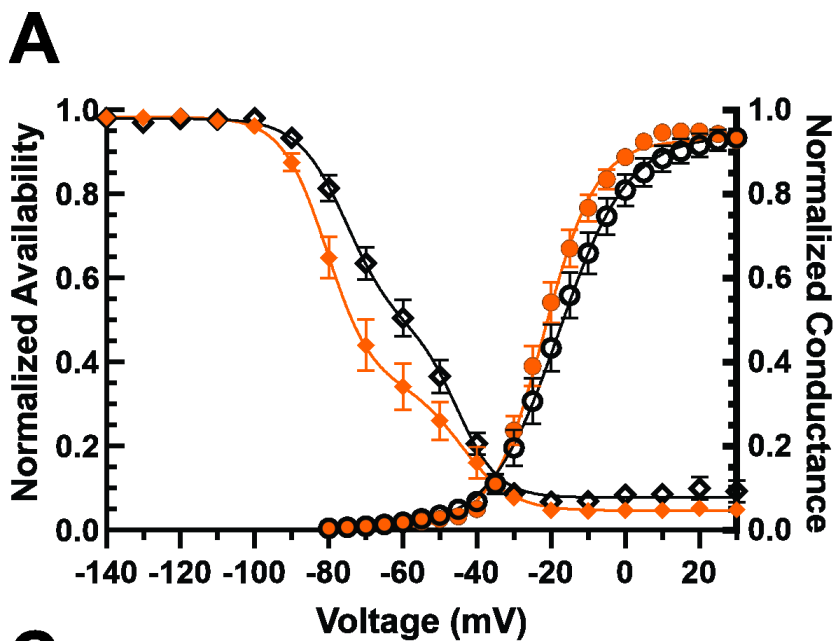
805 **Figure 5.** TTX-S current is upregulated in DRG neurons expressing Y69H β 2 subunits.
806 **(A)** Representative traces illustrating reference series subtraction to determine TTX-S
807 current (right) from the difference between total sodium current (left) and TTX-R current
808 (middle) recorded in $1\mu\text{M}$ TTX. Example traces are shown for sodium currents in both
809 neurons expressing the wild-type β 2 variant (top) and the Y69H variant (bottom,
810 orange). **(B)** There is a statistically significant increase in total sodium current passed by
811 DRG neurons expressing the Y69H variant compared to DRG neurons expressing the
812 wild-type β 2 subunit. **(C)** TTX-S sodium currents in DRG neurons are upregulated in the
813 presence of the Y69H variant (orange), relative to the wild-type (monochrome) β 2
814 subunit. However, there is no change in TTX-R sodium current. **(D)** The voltage-
815 dependence of $\text{Na}_v1.7$ channel inactivation (left; diamonds) is not statistically different
816 between HEK293 cells expressing the wild-type β 2 (monochromatic) and the Y69H
817 variant (orange) subunits. Additionally, the voltage-dependence of activation (right,
818 circles) is also not statistically different. **(E)** The Y69H variant does not significantly
819 upregulate $\text{Na}_v1.7$ current density in HEK293 cells stably expressing $\text{Na}_v1.7$ channels when
820 compared to the wild-type β 2 subunit.

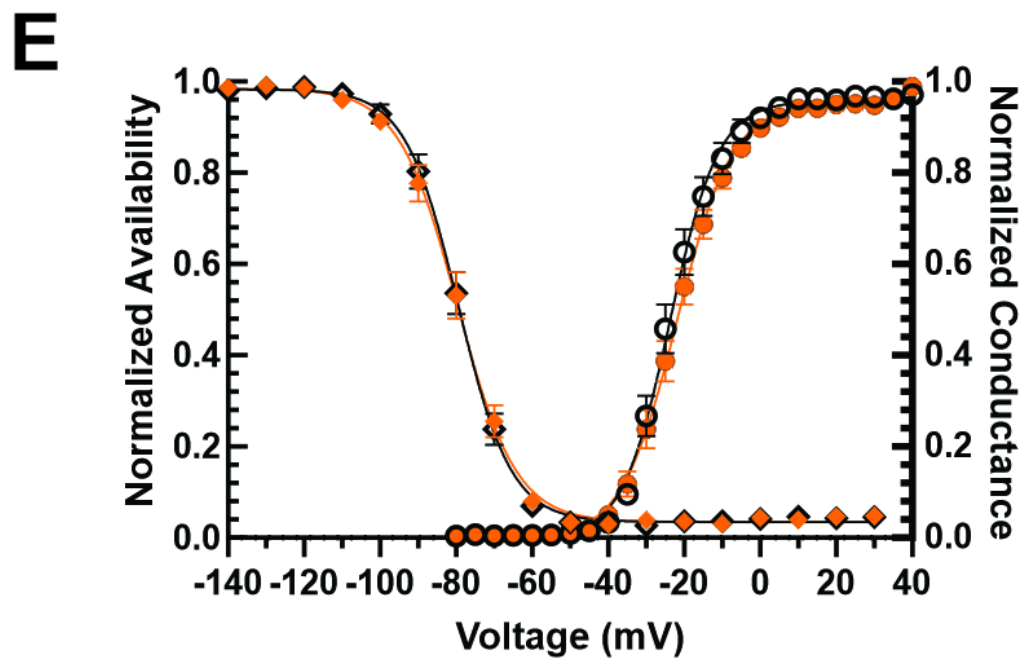
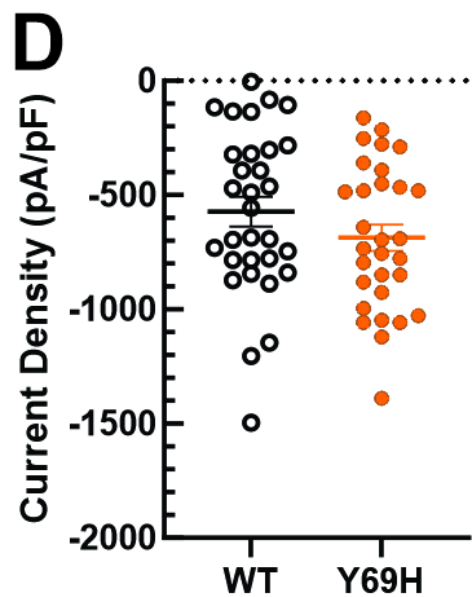
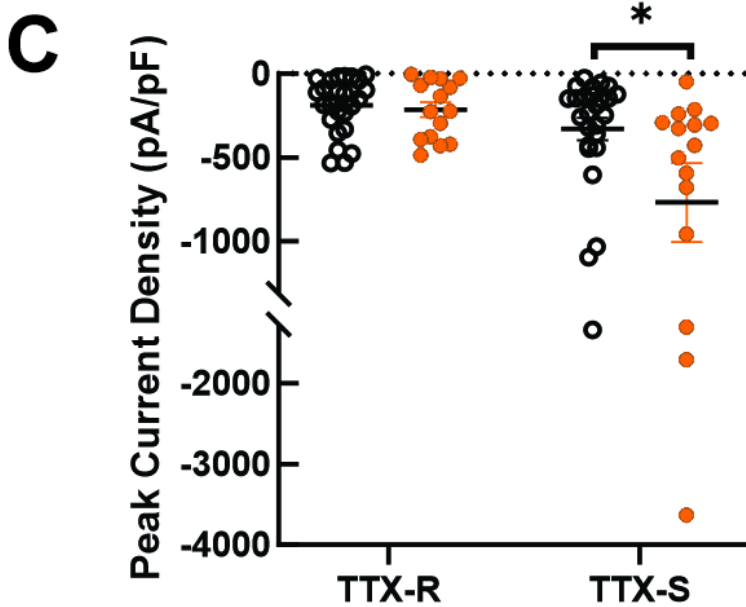
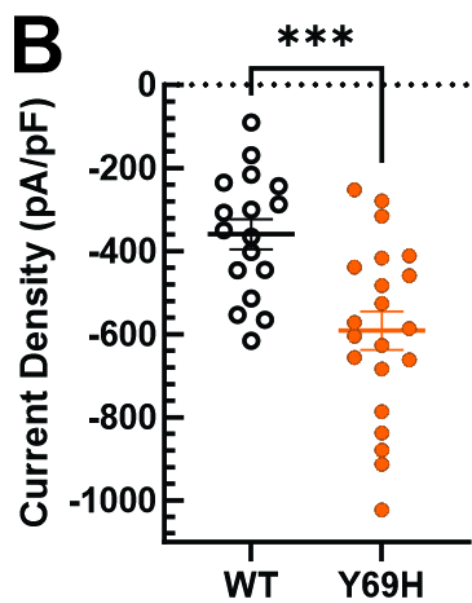
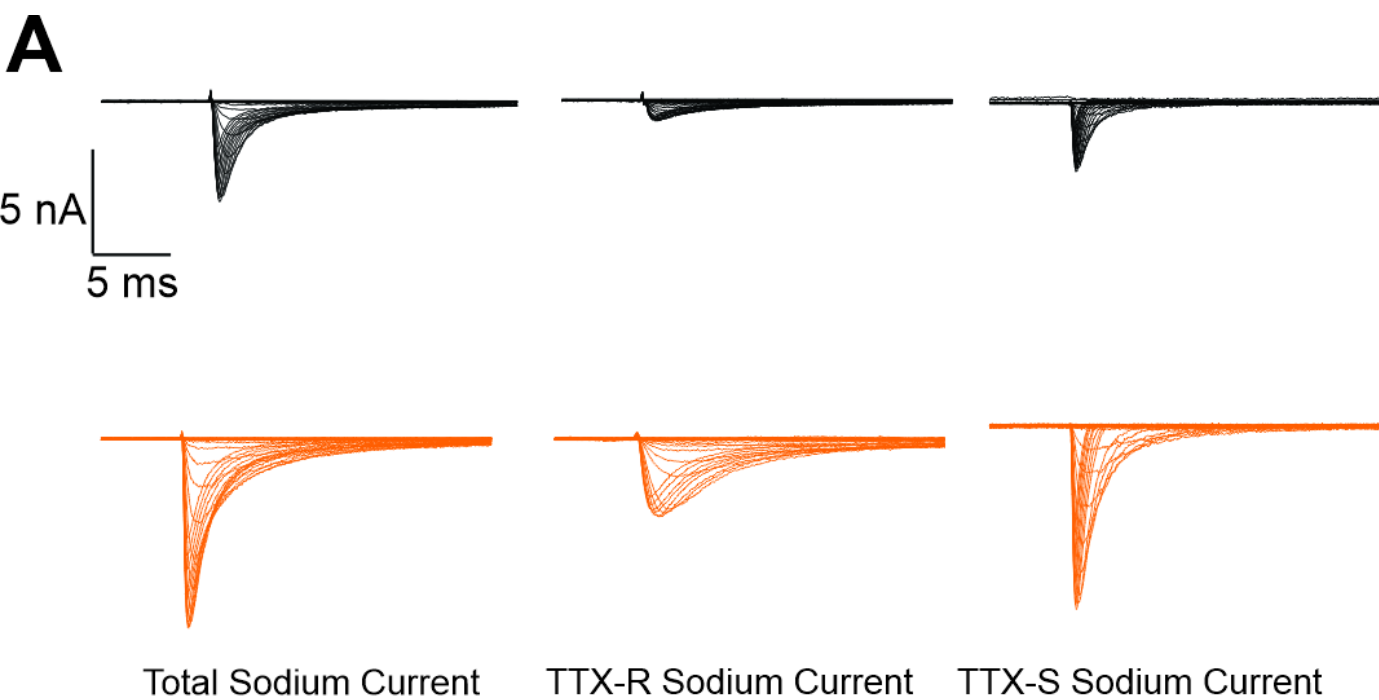
821 **Figure 6.** Schematic illustrating the proposed mechanism of action of the β 2-Y69H
822 (right) on small-diameter DRG neurons. Compared to the wild-type β 2 subunit (left),
823 neurons expressing the Y69H variant are hyperexcitable (top traces) and display a
824 larger TTX-S sodium current density (bottom traces), suggesting increased trafficking of
825 sodium channels to the neuronal membrane.





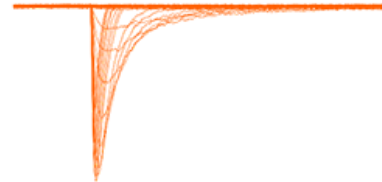
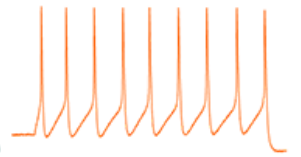
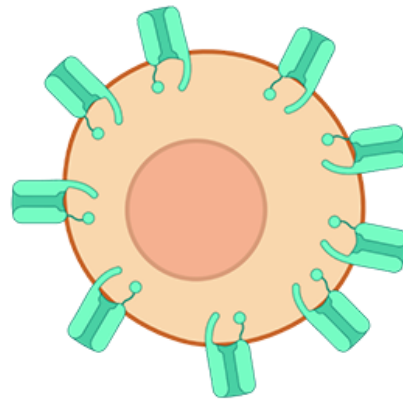
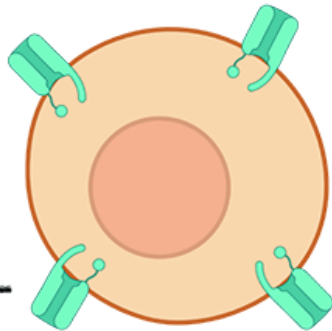






$\beta 2$ -Y69

$\beta 2$ -Y69H



$\beta 2$ -Y69

$\beta 2$ -Y69H

